THE ASTROPHYSICAL JOURNAL SUPPLEMENT SERIES, 80:369–401, 1992 May

ADIABATIC PROPERTIES OF PULSATING DA WHITE DWARFS. II. MODE TRAPPING IN COMPOSITIONALLY STRATIFIED MODELS

P. BRASSARD, G. FONTAINE, AND F. WESEMAEL
Département de Physique, Université de Montréal, C.P. 6128, Succ. A, Montréal, Québec, Canada H3C 3J7
AND
C. J. HANSEN
Joint Institute for Laboratory Astrophysics, University of Colorado, Box 440, Boulder, CO 80309
Received 1991 August 14; accepted 1991 October 11

ABSTRACT

As part of a series of investigations aimed at understanding the adiabatic gravity-mode period structure of models of pulsating DA white dwarfs, we examine qualitatively and quantitatively the phenomenon of mode trapping caused by compositional layering in these stars. This is motivated by the real possibility that the pulsation modes detected in ZZ Ceti stars are actually trapped in the outer hydrogen layer. We first discuss the various manifestations of compositional layering on the pulsational properties of a representative ZZ Ceti star model. The most important effect, from the point of view of the observations, is the formation of a *nonuniform* period distribution which bears the signature of the strength and location of the composition discontinuity. The trapped modes are conspicuous in that they show the largest deviations from the mean behavior in the period distribution, and are the most sensitive to the characteristics of the H/He composition transition zone. We thus derive a semianalytic formula relating the periods of trapped modes to model properties, which can readily be used to estimate the hydrogen layer mass in a ZZ Ceti star. We then use a more formal approach by investigating, in the asymptotic limit of high radial overtones, the effects of a true discontinuity (an idealization of the H/He transition zone in a DA white dwarf) in the Brunt-Väisälä frequency profile on the g-mode period spectrum of a stellar model. We find an analytic expression which gives the *full* period spectrum of the model in terms of only four parameters. As a by-product, we also derive another expression which gives, in terms of the same parameters, the period spectrum of trapped modes only. We show that these four parameters are related to the structural properties of a star. Comparisons with exact numerical calculations indicate that our first analytic expression accounts well for the essential features of mode trapping on the full period spectrum of a stellar model. Similar comparisons show that our second analytic expression reproduces quite *accurately* the period spectrum of trapped modes, raising the interesting prospect of being able to use a very simple model as a guide for interpreting observed period distributions in ZZ Ceti stars and for inferring some of their fundamental properties. On the basis of this simple asymptotic model, we finally propose a procedure for analyzing future observations of ZZ Ceti stars (the current data are not suitable for this type of analysis) in terms of mode trapping.

Subject headings: stars: interiors — stars: pulsation — stars: white dwarfs

1. INTRODUCTION

We have recently embarked on a series of investigations aimed at exploring the systematics of the adiabatic period structure of models of ZZ Ceti stars. These objects are ordinary DA white dwarfs confined to a narrow instability strip centered around $T_{\rm eff} \simeq 12{,}000$ K. They are undergoing multiperiodic luminosity variations which result from the superposition of excited nonradial pulsation modes of the g (gravity) type. More details on these fascinating stars as well as a discussion of the general goals of our ongoing study have been presented by Brassard et al. (1991a, hereafter Paper I).

Numerous previous investigations have demonstrated that the g-mode spectrum is formed in the outer layers of a white dwarf. Recently, however, this view has been challenged by some investigators, and it was one of the aims of Paper I to understand this difference. In the process, we have conclusively established that g-modes indeed probe the outer envelopes of white dwarfs. Hence, as previously believed, g-mode periods must be very sensitive to the details of the envelope structure in such stars. We have shown that the source of the confusion came from an inadequate treatment of the Brunt-Väisälä frequency in degenerate matter, and we have consequently provided a general expression appropriate for use in any type of stars. In particular, this expression is most useful in presence of composition gradients.

Because white dwarfs are expected to be compositionally stratified (with a thin layer of hydrogen on top of a thin layer of helium on top of a carbon-oxygen core in a typical DA white dwarf), and because g-modes have been shown to be sensitive to the envelope structure, it is clear that the period spectrum of a ZZ Ceti star must bear the signature of such stratification. Indeed, it is one of the stated goals of white dwarf seismology to infer how much hydrogen and helium are present on a ZZ Ceti star on the basis of its observed period spectrum.

A fundamental problem related to the interpretation of the observations has remained, however. A typical g-mode period spectrum computed from theory contains many modes over a

finite range in period, whereas most of these (especially for the low-amplitude variables) are *not* observed. Some of these unobserved modes may be associated with a sufficiently complex patchwork of light variations on the stellar surface that the variations would become unobservable (Dziembowski 1977; Brassard, Wesemael, & Fontaine 1991b), or some may have amplitudes below current limits of detectability. For the rest of the theoretically predicted modes, however, we need an exceptionally good filtering mechanism to explain why only a few modes, sometimes with high overtones, are selected in real stars.

Such a filtering mechanism was first proposed by Winget, Van Horn, & Hansen (1981), who considered *mode trapping* in the upper layers of compositionally stratified white dwarfs. They found that some modes resonate with the thickness of the hydrogen layer causing the pulsation wave energy to be reflected by the H/He interface; that is, they become trapped within the thin outer layer of hydrogen. Trapping is important because damping of g-modes in ZZ Ceti stars takes place in the core of these stars and, if fluid displacements cannot reach into the core, driving toward instability is enhanced. Subsequent nonadiabatic studies (Winget 1981; Dolez & Vauclair 1981; Winget et al. 1982; Winget & Fontaine 1982) have confirmed this by demonstrating that trapped modes have the most rapid growth rates, implying (but not proving) that the trapped modes are the most likely to be observed. This suggests that trapped modes could play a critical role in the interpretation of observations. To warn the reader, however, it should be pointed out that the suggested correlation between amplitude and trapping does not appear to hold for PG 1159−035, although this is *not* a ZZ Ceti star (Winget et al. 1991).

In this work, we take a closer look at the phenomenon of mode trapping in white dwarfs, bearing in mind the possibility that the actual observed modes could *all* be trapped modes. We note that some aspects of mode trapping in a ZZ Ceti star context have been discussed as part of numerous, mostly *numerical* investigations of the pulsation properties of white dwarfs (Winget et al. 1981; Dolez & Vauclair 1981; Winget 1981; Winget et al. 1982; Winget & Fontaine 1982; Wood & Winget 1988; Kawaler & Weiss 1991; Fontaine et al. 1991a; Bradley & Winget 1991; Kawaler 1991; Brassard et al. 1991c, d). However, a complete and detailed description of the various manifestations of mode trapping in ZZ Ceti stars has not yet been presented, and it is the first goal of the present paper to fill that need. Thus, in the next section, we present the various manifestations of mode trapping in a representative compositionally stratified white dwarf model. The second goal of this paper is to develop a better physical understanding for that aspect of mode trapping which bears directly on the observations, namely, its effects on the period spectrum itself. To this end, we first derive, in § 3, a semianalytic formula for the periods of trapped modes which is expressible in terms of model parameters. In the next section we present a more formal approach to the phenomenon of mode trapping in white dwarfs through the use of asymptotic theory. Specifically, we use the detailed asymptotic expressions of Tassoul (1980) to investigate the effects of a discontinuity in the Brunt-Väisälä frequency (caused by a composition gradient or some other cause) on the period spectrum. We then compare, in § 5, the predictions given by this analysis to the results of detailed numerical calculations. In § 6 we present a procedure based on our asymptotic model for interpreting the observations of ZZ Ceti stars in terms of mode trapping. Finally, we summarize our results in § 7.

2. THE PROPERTIES OF TRAPPED MODES

It is well established that the g-mode period spectrum of a star is intimately related to the spatial distribution of the square of the Brunt-Väisälä frequency. In Paper I we have shown that an appropriate expression of this quantity for use in models of degenerate stars is given by

$$N^2 = \frac{g^2\rho}{P}\frac{\chi_T}{\chi_\rho}(\nabla_{\rm ad} - \nabla + B)\,, \tag{1}$$

where g is the local gravity; ρ is the density; P is the pressure; $\chi_T = (\partial \ln P/\partial \ln T)_\rho$ and $\chi_\rho = (\partial \ln P/\partial \ln \rho)_T$ are the usual logarithmic pressure derivatives with respect to temperature and density, respectively; $\nabla_{\rm ad}$ is the adiabatic temperature gradient; and ∇ is the actual temperature gradient. The term B is given by

$$B = -\frac{1}{\chi_T}\left(\frac{\partial \ln P}{\partial \ln Y}\right)_{\rho,T}\frac{d \ln Y}{d \ln P}\,, \tag{2}$$

where Y is the mass fraction of helium, which uniquely specifies the local chemical composition in compositionally layered models of white dwarfs with H/He and He/C transition regions. The term B gives the explicit contribution of a change of chemical composition to the Brunt-Väisälä frequency. In white dwarf models this quantity is always positive and assumes (in presence of diffusive equilibrium) nonnegligible values *only* in regions where the abundances of the two atomic species are comparable, i.e., in the composition transition zones themselves (see Paper I).

The solid line in Figure 1 illustrates the run of the square of the Brunt-Väisälä frequency versus depth in a typical ZZ Ceti star model. This particular model has been selected from the 60210L1 sequence of Tassoul, Fontaine, & Winget (1990), and consists of a 12,518 K, $M_* = 0.6\ M_\odot$ object with a pure carbon core surrounded by a mantle containing $10^{-2}\ M_*$ of helium itself surrounded by a thin hydrogen envelope containing $10^{-10}\ M_*$. The composition gradients in the transition zones are computed under the assumption of diffusive equilibrium. Convection, which is present in the outermost hydrogen layers, is treated with the standard model of Böhm-Vitense (1958). Note that our choice of the abscissa ($\log q \equiv \log [1 - M(r)/M_*]$) strongly emphasizes the outer layers; it is only in these outer regions that g-modes have nonnegligible amplitudes in white dwarfs. The value $\log q = 0$ corresponds to the center of the star, and large negative values of $\log q$ correspond to the photospheric layers.

Apart from the general decrease toward the interior associated with increased degeneracy, the N^2 distribution of our reference model shows two striking features. The first one is the spike which is centered on $\log q \approx -10$ and which corresponds to the term B associated with the change of chemical composition in the H/He transition zone. Our model properly takes into account the phenomenon of (ordinary) diffusion,

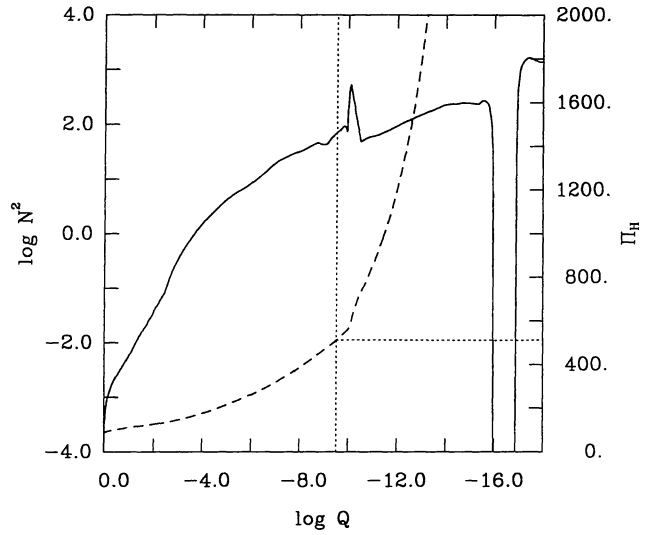

FIG. 1.—Square of the Brunt-Väisälä frequency as a function of fractional mass depth for our reference model (*solid curve*). The dashed line shows the running integral Π_H as function of depth; the values of Π_H are to be read on the right-hand axis. The vertical and horizontal dotted lines show, respectively, the location of the effective H/He interface and its associated value of Π_H.

and this leads to a composition transition zone of finite extent (as opposed to a true discontinuity in composition). Hence, the spike in N^2 has a finite width, and its actual shape and strength are important in determining the period structure of the model. Note that, in order to avoid as far as possible the complications of double-resonance conditions in what follows, we have minimized the effects of the He/C transition zone by explicitly taking $B = 0$ in that region. The small kink in the N^2 curve that can be observed around $\log q \simeq -2.5$ is what is left of this operation. It represents small, residual effects of changing the chemical composition in that region.

The second feature is the well in the N^2 distribution corresponding to convectively unstable regions (in which $N^2 < 0$) due to partial ionization of hydrogen in the outermost layers. The presence of the quasi-discontinuities in N^2 associated with the thin hydrogen convection zone, the H/He spike at $\log q \simeq -10$, and even the small feature at $\log q \simeq -2.5$ are directly responsible for the filtering capabilities of the model. Indeed, as discussed in Paper I, *any* discontinuity or quasi-discontinuity in the N^2 distribution leads to resonance conditions which may trap modes in various regions of a model. The potential for mode trapping does not exist in a chemically homogeneous radiative model, and N^2 is smooth and continuous in that case.

In practice, mode trapping due to the presence of a superficial hydrogen convection zone in a ZZ Ceti star model occurs only for *g*-modes with periods much larger than those thus far observed in real pulsators. Thus, in what follows, we will focus primarily on the effects of mode trapping caused by composition transition zones and, in particular, those caused by the H/He buffer region in our reference model. Note, however, that the analytic model which will be developed below can be transposed directly to the case of trapping due to a small convection zone or other possible causes.

A mode which is trapped in the outer layers of a white dwarf is characterized by a relatively low value of its global kinetic energy defined by

$$E_{\rm kin} = \frac{1}{2}\sigma^2 \int_V |\delta \boldsymbol{r}|^2 \rho \, dV , \qquad (3)$$

where σ is the eigenfrequency, V is the total volume, ρ is the density, and $\delta \boldsymbol{r}$ is the Lagrangian displacement vector. Figure 2 shows the normalized (with $\delta r/r|_{\rm surface} = 1$) kinetic energy of a mode as a function of the period for our reference model. Each plotted point corresponds to a radial overtone starting to the left with $k = 1$ for *g*-modes with $l = 1$, 2, and 3 and periods less than 1400 s. We have used the new adiabatic code of Brassard et al. (1992) based on a finite-element method of the Galerkin type to solve the eigenvalue problem for our reference model. In this particular computation, we have described the model in terms of 10,000 quadratic elements, sufficient to have an error less than 0.0001% in the period of an $l = 3$, $k = 50$ mode. We have considered modes with periods up to 4000 s, but we only illustrate here the period window of direct relevance to the observed periods in real ZZ Ceti stars.

The minima in the curves shown in Figure 2 correspond to modes which are trapped in the region above the H/He interface. A comparison with Figure 5 of Paper I indicates that secondary minima and structure associated with mode trapping caused by the much deeper He/C transition zone have largely disappeared here through our choice of $B = 0$ for that region. Our present results are therefore "cleaner" (but less realistic) than those obtained from models in which both the H/He and He/C transition regions are treated properly. This is done on purpose here, of course, because it facilitates the comparison with the analytic model to be discussed below. Note also that the H/He transition zone has a finite width imposed by diffusion considerations, and, therefore, certain modes (particularly those immediately adjacent to a mode showing a minimum in kinetic energy) could be thought of as *partially trapped.* In addition, our description of the H/He transition zone in terms of diffusive equilibrium implies that no special treatment of that zone is needed from the pulsation point of view. The composition may change quickly in that zone, but it does so *smoothly.* By contrast, it is necessary to use special "jump" conditions at the H/He interface in those models which are characterized by true composition discontinuities (see Winget et al. 1981). Otherwise, mode trapping may be completely missed in the numerical calculations. Qualitatively, the two approaches give the same results, but there are substantial differences from a quantitative point of view, since the details of mode trapping (the exact structure of a kinetic energy-period diagram for example) depend on the details of the composition variation in the transition zone.[1]

Figure 3 illustrates the distribution of the *kinetic energy density* (the integrand of eq. [3] plotted on an arbitrary scale) for

[1] In this connection, it should be pointed out that a numerical glitch is responsible for the contrast of many orders of magnitude between the kinetic energy of the first trapped mode in Fig. 2 of Winget et al. (1981) and the kinetic energies of its adjacent modes (M. A. Wood 1989, private communication). In reality, mode trapping in their model does lead to a kinetic energy which behaves a lot more like the results in our Fig. 2 or, perhaps more appropriately because He/C trapping is included there, like the results in Fig. 5 of Paper I.

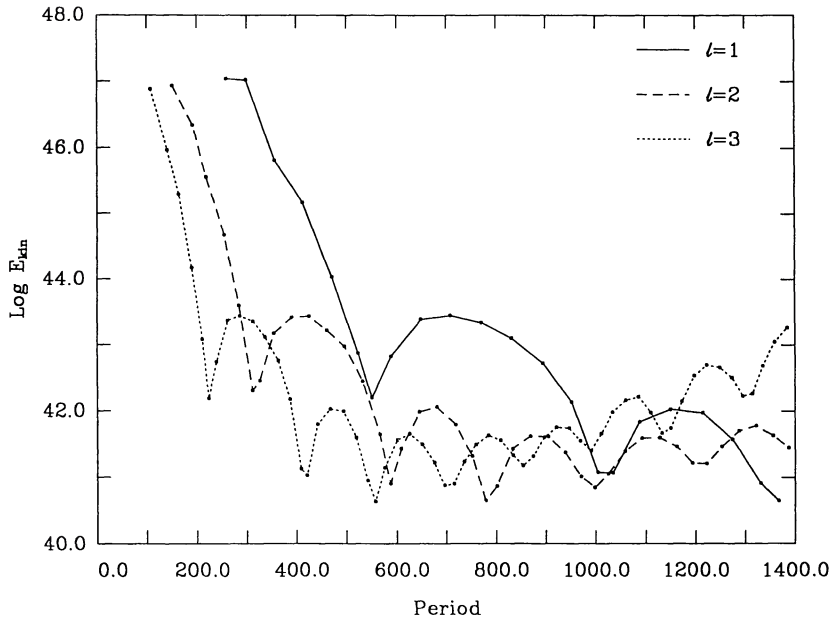

FIG. 2.—Kinetic energy vs. period for all g-modes of our reference model in the period range 0 s $\leq P \leq$ 1400 s and with $l = 1$ (*solid curve*), $l = 2$ (*dashed curve*), and $l = 3$ (*dotted curve*). Each plotted point corresponds to a radial overtone starting to the left with $k = 1$ for all three curves.

three consecutive overtones with $l = 3$ in our reference model. The modes shown have $k = 6$ (*solid line*), corresponding to a trapped mode showing a minimum in kinetic energy in Figure 2; $k = 7$ (*dotted line*), its adjacent mode showing higher energy and which could be considered as partially trapped, and $k = 8$ (*dashed line*), a mode with still higher kinetic energy. It is apparent that the kinetic energy density of a trapped mode is considerably reduced below the H/He transition region around $\log q \simeq -10$. The results illustrated here are quite typical of other trapped modes in our model.

In terms of the Dziembowski (1971) variables, the kinetic energy of a mode depends on the eigenfunction y_1, which is related to radial displacements, and on the eigenfunction y_2, which measures transverse displacements. In white dwarf stars the total displacement is dominated by horizontal motions, which implies that the kinetic energy of a mode is largely specified by the behavior of y_2. Thus, the minima shown in the curves of Figure 3 correspond to the nodes of y_2. These minima are not zero, however, because y_1 still contributes to the energy, and its nodes do not fall on those of y_2.

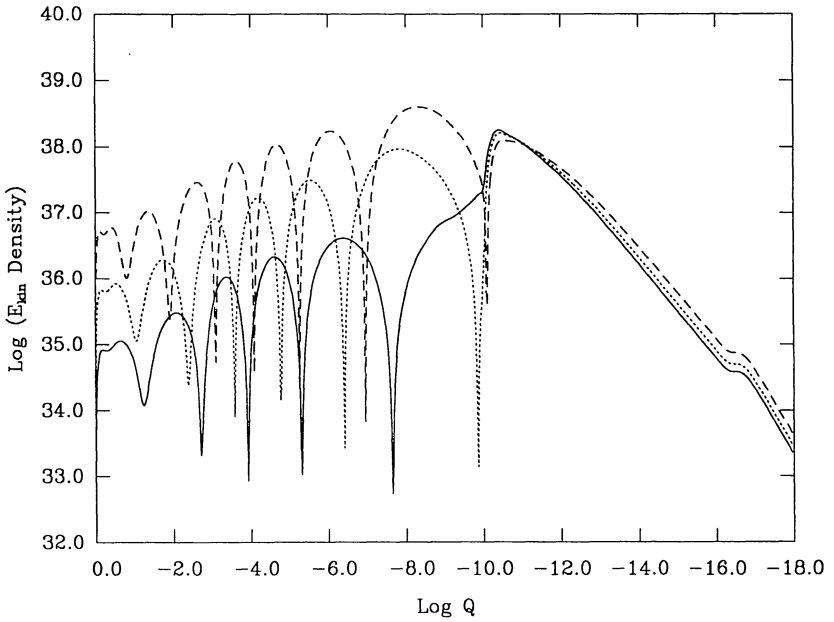

FIG. 3.—Kinetic energy density (arbitrary scale) in terms of depth for three consecutive g-modes with $l = 3$: $k = 6$ (*solid curve*), $k = 7$ (*dotted curve*), and $k = 8$ (*dashed curve*).

Figures 4*a* and 4*b* show, respectively, the behavior of the normalized eigenfunctions y_1 and y_2 for the same three modes with $l = 3$ and $k = 6$, 7, and 8 as a function of depth in our model. Note the very important general decrease of the eigenfunction amplitudes of all modes toward the interior, indicating how fluid motion is restricted to the outer nondegenerate envelope in a white dwarf. Note also that the amplitudes (y_1 and y_2) of the trapped mode ($k = 6$) are reduced considerably below the H/He transition zone, as compared, for example, with a more "normal" mode such as the one with $k = 8$. Of course, it is the reduction of the amplitudes of the eigenfunctions below the H/He transition zone (particularly y_2 here) which is directly responsible for the decrease in the kinetic energy of a trapped mode, since the latter is proportional to the displacement vector integrated over the whole star (see eq. [3]). This relative reduction is also the essence of the filtering mechanism proposed by Winget et al. (1981): trapped modes are less damped than other modes because damping takes

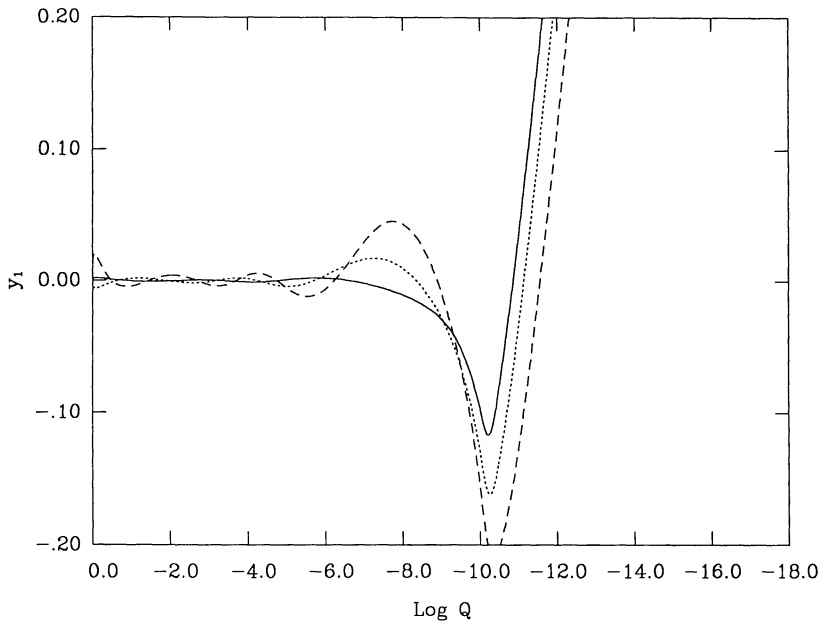

FIG. 4*a*

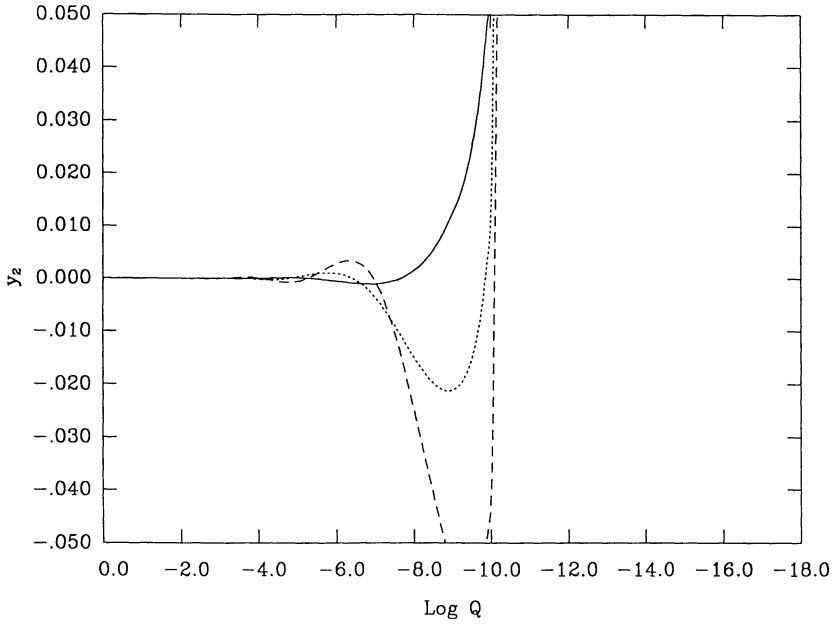

FIG. 4*b*

FIG. 4.—(*a*) Normalized eigenfunction y_1 vs. fractional mass depth in our reference model for three consecutive *g*-modes with $l = 3$: $k = 6$ (*solid curve*), $k = 7$ (*dotted curve*), and $k = 8$ (*dashed curve*). (*b*) Same as (*a*), but for the eigenfunction y_2.

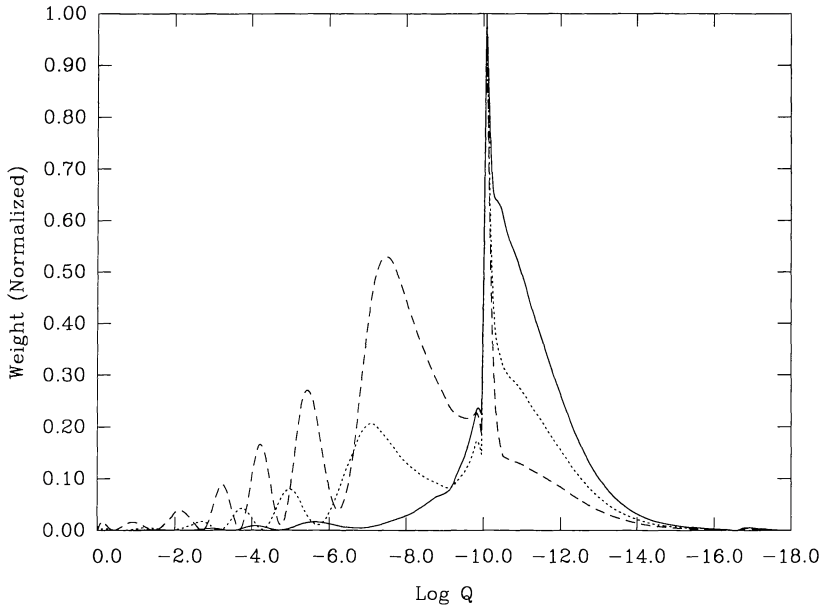

FIG. 5*a*

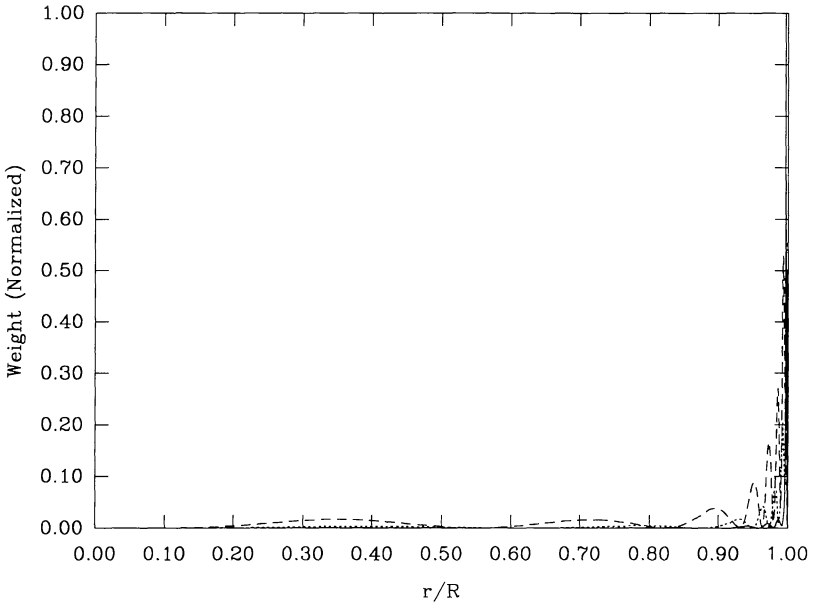

FIG. 5*b*

FIG. 5.—(*a*) Normalized weight function vs. fractional mass depth in our reference model for three consecutive *g*-modes with $l = 3$: $k = 6$ (*solid curve*), $k = 7$ (*dotted curve*), and $k = 8$ (*dashed curve*). (*b*) Same as (*a*), but the abscissa is given in terms of the radial coordinate. The figure explicitly shows how periods are formed in the outermost layers in white dwarfs. (*c*) Same as (*b*), but with a blowup of the outermost regions.

place in the cores of white dwarfs, in regions where their eigenfunction amplitudes have been significantly reduced as compared with these other modes. This enhances driving, which suggests that trapped modes should be selectively excited and observed. In this context, the contrast in kinetic energy between consecutive modes can be thought of as a rough measurement of the "efficiency" of this selection process. Presumably, trapped modes which show large differences in kinetic energy with respect to their adjacent modes (the low-period modes at the bottom of the sharp minima in Fig. 2, for example) should be filtered out more easily than trapped modes which show relatively small differences in kinetic energy with their neighboring modes.

The location of the H/He transition zone bears directly on the question of the efficiency of the mode selection mechanism. Clearly, the contrast in kinetic energy between a trapped mode and its adjacent modes can be the largest when the composition transition zone is located in the outermost layers. For models with relatively thick hydrogen layers, the H/He transition zone would be located in a deep, highly degenerate region,

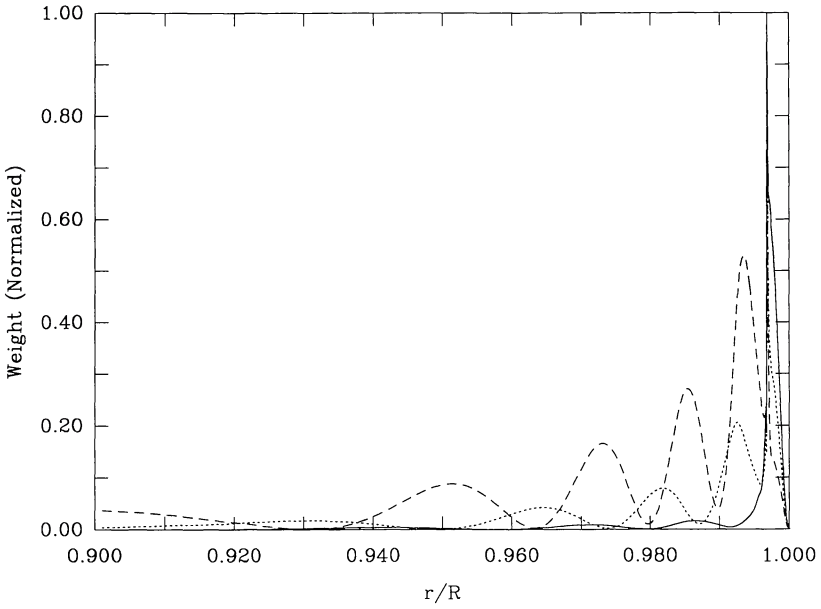

FIG. 5*c*

where the eigenfunction amplitudes would already be quite small precisely because of the degenerate environment. In such cases, the differences in the kinetic energy integral between various modes would not be very large. The detailed numerical calculations of Brassard et al. (1991d) using models with many values of the outer hydrogen layer mass show that this is indeed the case. Thus, we could say that a ZZ Ceti star model progressively loses its ability to select (trapped) modes as its hydrogen layer mass is increased. Note, however, that, contrary to the case of the kinetic energy discussed here, mode trapping due to composition layering always keeps a distinct imprint on the period spectra of models, even those with thick hydrogen layers (see below).

Figures 4*a* and 4*b*, and additional ones (not shown here), further reveal that the presence of the H/He transition zone produces a "pinching" effect on the eigenfunctions of *all* modes. This means that all of the periods are affected, and, therefore, for all modes, some weight of period formation must come from the H/He transition region. This is clearly illustrated in Figure 5*a,* where we present the normalized weight functions (as defined in Kawaler, Hansen, & Winget 1985) for our three modes of interest. Figures 5*b* and 5*c* show the same, but on a radius scale. Such functions give the relative contributions of the different locations in the star to the period formation. We can observe that, for the trapped mode (*solid line*), the period is essentially formed in the range $-9 \gtrsim \log q \gtrsim -13$, much higher than the $k = 8$ mode whose period is formed in the considerably larger depth range $-3 \gtrsim \log q \gtrsim -12$. As a rule, trapped modes probe much higher in the envelopes of white dwarfs than normal modes, generally above the H/He trapping region. Nevertheless, Figure 5*a* also indicates that the H/He transition zone is of some importance in the period determination of the other modes ($k = 7$ and 8) as well, because the maxima of the weight functions are all at a value near $\log q \simeq -10$. Hence, the complete period spectrum must be affected by the presence of composition transition layers in ZZ Ceti stars.

A detailed examination of the eigenfunctions in our reference model (and in many others) also leads to a qualitative but very general and useful result as to the conditions for mode trapping. Indeed, we can observe that in a given model, and for given l, the nodes of y_1 and y_2 are pushed toward the surface when k increases. Moreover, a node in y_1 is always located above the *corresponding* node in y_2. Starting with $k = 1$, for example, we generally find that the first node (counted from the surface) in both y_1 and y_2 is located below the H/He transition zone. Upon increasing k, we eventually find two or three consecutive modes such that the first node in y_1 has crossed the H/He interface from below, while the corresponding node in y_2 is still just below that interface. Such modes correspond to the first trapped mode accompanied by one or two of its immediate neighbors (partially trapped modes). For the next higher value of k, the first node in *both* y_1 and y_2 will have crossed the H/He interface from below and the mode will behave more "normally" than the previous ones. For still higher values of k, the pattern repeats itself and one finds the second trapped mode, and so on. Thus, we find a useful general diagnostic for mode trapping on the basis of the eigenfunctions: *a mode can be considered trapped (or nearly so) above the* H/He *transition zone when its eigenfunction* y_1 *has a node just above the* H/He *interface while, at the same time, the corresponding node in* y_2 *lies just below that interface.* This combination of circumstances maximizes the reduction of the eigenfunction amplitudes below the composition transition zone. Note in passing that for large values of k, the distance between consecutive nodes of an eigenfunction become comparable and even smaller than the thickness of the H/He transition zone. In that case, the eigenfunctions of consecutive modes do not differ very much, even below the composition transition zone, and "mode trapping" does not apply to an isolated mode. Thus,

the contrast in kinetic energy between "trapped" and adjacent modes is considerably reduced, as can be observed in Figure 2 for high-period modes.

Qualitatively speaking, mode trapping should then occur when $y_1 \simeq 0$ (from above) at the H/He interface and $y_2 \simeq 0$ (from below) in the same region. The radial wavelength is then in resonance with the thickness of the outer hydrogen layer. Of course, it is not strictly possible to have both eigenfunctions vanish at the same location because their nodes do not coincide. Nevertheless, for a rough qualitative understanding of the phenomenon and for discussions of simplified models of trapping, the conditions $y_1 \simeq y_2 \simeq 0$ are useful (see next section). In addition, it is somewhat difficult to define here an "interface," since the H/He transition zone has a finite width. From a detailed examination of the behavior of the eigenfunctions, and, again, from a qualitative point of view, we find empirically that the appropriate "interface" is located just below the H/He spike in the Brunt-Väisälä frequency (see Fig. 1). For our reference model, the effective interface (from the point of view of the eigenfunctions) is located near $\log q \simeq -9.5$.

A look back at Figures 4*a* and 4*b* illustrates some of the points we just discussed. For example, for both the modes with $k = 7$ and 8, we see that y_1 *and* y_2 have *one* node above $\log q \simeq -9.5$. By contrast, the mode with $k = 6$ has *one* node in y_1 and *no* node in y_2 above the interface. The first node in y_2 is located below the interface. The same is true for the mode with $k = 5$ (not illustrated), while the mode with $k = 4$ (also not illustrated) has no node in both y_1 and y_2 above the interface. These last two modes show (as for the $k = 7$ and 8 modes) higher eigenfunction amplitudes than the trapped mode ($k = 6$) below the interface.

Another manifestation of mode trapping, which, however, we shall not dwell upon, is its effects on the first-order adiabatic rotation coefficient C_{kl} defined, for example, by Cox (1980, § 19.1*c*). This quantity measures the strength of frequency splitting for a $2l + 1$ degenerate mode of order k due to uniform rotation. The detailed numerical study of Brassard et al. (1991d) shows that trapped modes have generally the highest values of the coefficient C_{kl}. This is related to the fact that trapped modes are formed higher in the envelopes of white dwarfs. Indeed, for surface modes, Brickhill (1975) has shown that C_{kl} takes its largest value, which is given by the asymptotic value $1/[l(l + 1)]$. Thus, trapped modes usually show maxima in C_{kl}, but this correlation is somewhat looser than that shown between trapped modes and minima in kinetic energy. Nevertheless, the former property is useful for identifying trapped modes in numerical calculations when the contrast in kinetic energy between trapped and adjacent modes becomes small. This occurs, for example, and as mentioned above, when the hydrogen layer thickness becomes large (see Brassard et al. 1991d).

So far, we have focused our discussion of mode trapping in terms of model quantities. From the point of view of the observations, however, the most interesting manifestation of mode trapping due to composition layering lies with its effect on the period spectrum itself. Mode trapping in ZZ Ceti star models produces a *nonuniform period distribution* whose detailed structure depends on the location of the transition zone and the actual composition profile in that zone. A typical example is shown in Figure 6, where, on the basis of our reference

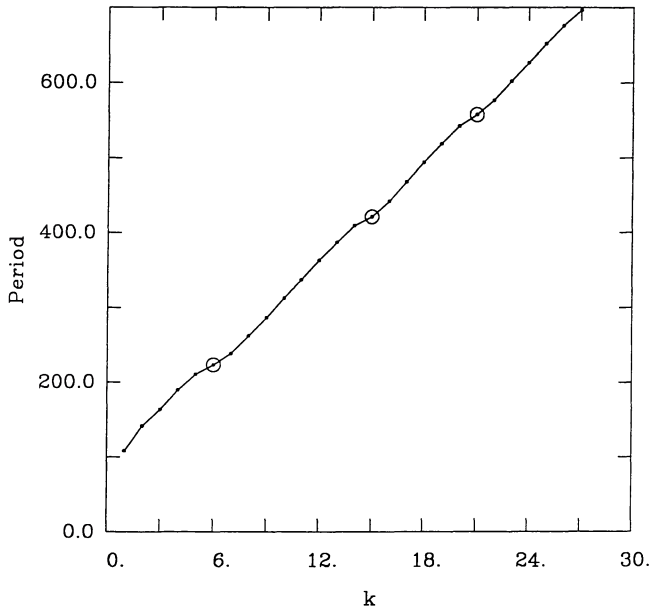

FIG. 6.—Period distribution (period vs. k) for the low-order $l = 3$ modes in our reference model. The circled dots identify the first three trapped modes.

model, we have plotted the periods of the first several modes with $l = 3$ in terms of k, the radial order. Circled dots identify the first three modes which are trapped and which belong to the $l = 3$ sequence (see, as a cross-reference, the dotted line in Fig. 2). For radiative models with uniform composition, asymptotic theory (see, e.g., Tassoul 1980) predicts a constant period spacing for sufficiently large values of k, thus leading to a straight line in Figure 6. We can observe significant deviations from this predicted linear behavior, particularly in the neighborhood of trapped modes, where there is a tendency for periods to be grouped together.

The nonuniformity of the period distribution is best observed in Figure 7, where, this time, we plot the period difference $\Delta P = P_{k+1} - P_k$ against P_k for the $l = 3$ modes. The solid line corresponds to our reference model, while the dotted line corresponds to the complete model in which the He/C transition zone has been treated properly. We show this here only as an illustrative example of the effects of trapping due to *both* the He/C and the H/He transition zones on the period spectrum. We can see that the dotted line has considerably more structure than the solid line. There are secondary minima which are more frequent than the primary minima, and which correspond to trapped modes at the He/C interface. Mode trapping there is weaker (the minima are less pronounced) because the He/C transition zone is located much deeper than the H/He transition zone, in a region where the weight functions are relatively small and the contrast between molecular weights is less than that between hydrogen and helium. In both models, the primary minima correspond to the modes trapped above the H/He transition zone, and, therefore, these minima correlate with the minima in kinetic energy observed in Figure 2. Note that with our definition of ΔP the actual minimum positions in Figure 7 are occupied by either trapped modes or modes which are immediately adjacent to them ($\Delta k = -1$).

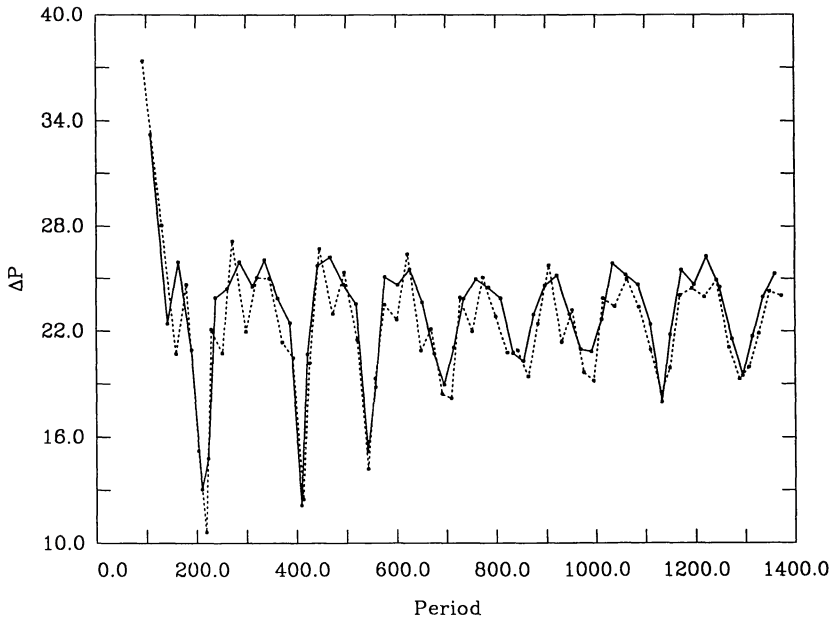

FIG. 7.—Period distribution (period spacing vs. period) for the $l = 3$ modes of two models in the 0–1400 s window. The solid line refers to our reference model, while the dotted line corresponds to the same model but with the full inclusion of the term B in the He/C transition zone.

The phenomenon of "period bunching" is obviously apparent in the neighborhood of trapped modes. Note also that the minima are more pronounced for the first few trapped modes. As mentioned above, the eigenfunctions of trapped and adjacent modes can differ considerably at low values of k, until the distance between two consecutive nodes becomes comparable to and, eventually, smaller than the H/He transition zone thickness for high-k modes. Our computations which we have carried out for modes with periods up to 4000 s in our reference model (corresponding to modes up to $k = 168$, $l = 3$) reveal that the nonuniformity of the period spectrum persists up to these large periods. The full period distribution resembles closely that shown in Figure 7 for $P_k \gtrsim 600$ s, with a pattern roughly repeating itself at regular intervals. We will show below that the cycle period of this pattern depends directly on the hydrogen layer mass. *Thus, we can conclude that the period spectrum of a ZZ Ceti star is dominated by mode-trapping effects, especially those caused by the presence of a* H/He *transition zone in the envelope.*

A final remark concerns the secondary structure shown in the solid curve in Figure 7. It should be said in this context that this differential diagram is an extremely sensitive method for presenting the results. We believe that the accuracy of our computations is sufficiently high that the secondary features observed in the curve are actually *real.* We are convinced that these features are caused by small, residual structure in the Brunt-Väisälä frequency occurring in the deep envelope of our reference model, particularly the small kink observed near $\log q \simeq -2.5$ in the neighborhood of the He/C transition region.

In the remainder of this paper, we will concentrate on a further description of the effects of mode trapping on the period spectrum itself. As mentioned earlier, it is the period distribution which is important in terms of interpreting the observations, and this deserves further discussion.

3. A SEMIANALYTIC FORMULA FOR THE PERIODS OF TRAPPED MODES IN LAYERED WHITE DWARF MODELS

It is possible to obtain crude estimates of the periods of g-modes trapped in the outer hydrogen layer of a compositionally stratified white dwarf envelope through the use of polytropes. Thus, we assume that the material in the hydrogen layer has a polytropic structure of the form

$$P = K\rho^{1+1/n}, \tag{4}$$

where P is the pressure, ρ is the density, K is a constant, and, as usual, n is the (constant) polytropic index.

In terms of Dziembowski's (1971) variables (and see Unno et al. 1989, § 18.1), the adiabatic wave equation in the Cowling approximation can be written

$$r\frac{dy_1}{dr} = \left[\frac{l(l+1)g}{rL_l^2} - 3\right]y_1 + \frac{l(l+1)g}{r}\left[\frac{1}{\sigma^2} - \frac{1}{L_l^2}\right]y_2, \tag{5}$$

$$r\frac{dy_2}{dr} = \frac{r}{g}(\sigma^2 - N^2)y_1 + \left[1 - U + \frac{r}{g}N^2\right]y_2, \tag{6}$$

where y_1 is related to the Lagrangian radial displacement, ξ_r, by $y_1 = \xi_r/r$, and y_2, which measures the transverse displacement, is proportional to the Eulerian variation of the pressure, P', through $y_2 = P'/\rho gr$. $U = 3\rho/\langle\rho\rangle$ and $V = \rho gr/P$ are the dimensionless variables of the U-V plane (Cox & Giuli 1968, § 21.4), and N^2 and $L_l^2 = l(l+1)g\Gamma_1/rV$ are, respectively, the squares of the Brunt-Väisälä and Lamb frequencies, with N^2 given by

$$N^2 = -g\left(\frac{1}{\rho}\frac{d\rho}{dr} - \frac{1}{\Gamma_1 P}\frac{dP}{dr}\right). \tag{7}$$

Note that equation (1) is actually a transformed version of this

last equation, where the transformation must be performed in numerical pulsation calculations of degenerate stars (see Paper I). The eigenfrequency σ is in units of radians per second and is the result of the temporal decomposition $e^{i\sigma t}$. As usual, the angular momentum quantum number l (from the spherical harmonics, Y_l^m) may take on only nonzero positive integer values for nonradial modes.

The pulsation equations (5) and (6) may be simplified considerably by using the following approximations appropriate to the outer layer of a ZZ Ceti star undergoing g-mode oscillations: $U \approx 0$, $|N^2| \gg 1$, $V \gg 1$, and $\sigma^{-2} \gg 1$. The resulting equations can then be recast in our polytropic model for the hydrogen layer as

$$r\frac{dy_1}{dr} = \frac{r\tilde{n}}{R-r}y_1 + \left[\frac{l(l+1)}{\omega^2} - \frac{r\tilde{n}}{R-r}\right]y_2 , \tag{8}$$

$$r\frac{dy_2}{dr} = -\frac{r}{R-r}(n-\tilde{n})(y_1 - y_2) , \tag{9}$$

where we have introduced the dimensionless frequency $\omega^2 = r\sigma^2/g$ and $\tilde{n} = (n+1)/\Gamma_1$. Note that in the outer layers r/g is approximately a constant equal to R^3/GM.

These equations are now transformed by defining the new independent variable x by

$$x^2 \equiv \frac{4(n-\tilde{n})l(l+1)}{\omega^2}\frac{R-r}{R} , \tag{10}$$

where we assume that $n > \tilde{n}$. This last assumption is equivalent requiring that the stellar material is not convective. The pulsation equations now take on the form

$$x^2\frac{d^2y_2}{dx^2} + (2n+1)x\frac{dy_2}{dx} + x^2y_2 = 0 \tag{11}$$

and

$$y_1 = \frac{x}{2(n-\tilde{n})}\frac{dy_2}{dx} + y_2 , \tag{12}$$

where advantage has been taken of the fact that we are high in the envelope ($r/R \approx 1$). Solutions are given by

$$y_2 = x^{-n}[C_1J_n(x) + C_2Y_n(x)] \tag{13}$$

and

$$y_1 = y_2 - \frac{x^{1-n}}{2(n-\tilde{n})}[C_1J_{n+1}(x) + C_2Y_{n+1}(x)] , \tag{14}$$

where $J_n(x)$ and $Y_n(x)$ are the usual Bessel functions of the first and second kinds and C_1 and C_2 are constants of integration. In our simple model, the boundary conditions at the surface can be written $y_1 = y_2 = 1$ at $x = 0$ (normalization condition). The solution for the hydrogen layer is then given by equations (13) and (14) with constants of integration $C_1 = 2^n\Gamma(n+1)$, and $C_2 = 0$.

To proceed further, it would be necessary to discuss the matching of the solution we just found for the hydrogen layer with the corresponding solution for the helium layer at the H/He discontinuity as well as the boundary conditions at the center. However, for our present needs, it is sufficient to realize (see the previous section) that the conditions for trapping in the hydrogen layer require that $y_2 \simeq 0$ and $y_1 \simeq 0$ at the H/He interface. It is further shown below that these conditions are indeed legitimate. Hence, approximate values of the periods of trapped modes can be obtained by seeking the conditions such that

$$y_2 \propto J_n(x) = 0 \tag{15}$$

and

$$y_1 \propto \left[J_n(x) - \frac{xJ_{n+1}(x)}{2(n-\tilde{n})}\right] = 0 \tag{16}$$

at $r = r_H$, i.e., at the H/He interface. Strictly speaking, it is not possible to simultaneously satisfy these two conditions. However, to enumerate the eigenperiods crudely for trapped modes here, it is sufficient to satisfy these conditions independently. Each condition will, of course, lead to its own independent (and different) period spectrum for trapped modes. In the first case, the condition is satisfied for discrete values of x (we call them x_i) which correspond to the zeros of the Bessel function $J_n(x)$. In the other case, the condition is satisfied for other discrete values of x such that $x_i/[2(n-\tilde{n})] = J_n(x_i)/J_{n+1}(x_i)$. Using equation (10), we thus obtain the period spectrum of trapped modes in the outer hydrogen layer,

$$P_{il} = 2\pi\lambda_i\left[l(l+1)\left(1 - \frac{r_H}{R}\right)\frac{GM}{R^3}\right]^{-1/2} , \tag{17}$$

where, following the notation of Kawaler & Weiss (1991), we have introduced the "trapping coefficient" $\lambda_i \equiv x_i/[2(n-\tilde{n})^{1/2}]$. Here the index i corresponds to the order of the trapped mode in the hydrogen layer, i.e., it labels the number of nodes in y_1 above the H/He interface.

Typical values of the effective polytropic index in the radiative parts of the hydrogen envelopes of representative models of ZZ Ceti stars are usually found in the range 2–3. As an illustrative example, we take $n = 2.5$. Combined with $\Gamma_1 \simeq 5/3$ ($\tilde{n} \simeq 2.1$) and the properties of $J_{2.5}(x)$ and $J_{3.5}(x)$, we find the first few values of the trapping coefficient: $\lambda_1 = 1.82$ (4.56), $\lambda_2 = 5.75$ (7.19), and $\lambda_3 = 8.29$ (9.76) on the basis of condition (16) (condition [15]). Not unexpectedly, these values correspond to periods for trapped modes which do not match very well the periods obtained from actual pulsation calculations. Nevertheless, these numbers are not unlike those obtained by Kawaler & Weiss (1991; see also Kawaler 1991), who have cleverly suggested that a much better match would be achieved by keeping the general form provided by equation (17), doing away with the λ_i coefficients estimated on the basis of Bessel functions, and replacing them by actual fits to detailed pulsation results. In this way, they have obtained average values of λ_i which, perhaps surprisingly, show little dispersion with model parameter changes. On the basis of their own models,

TABLE 1

AVERAGE VALUES OF TRAPPING COEFFICIENTS FOR ZZ CETI STAR MODELS

Source	λ_1	λ_2	λ_3	λ_4	λ_5	λ_6
Kawaler & Weiss 1991[a]	2.21 ± 0.06	4.38 ± 0.06	6.06 ± 0.20	7.59 ± 0.20	9.07 ± 0.20	10.50 ± 0.30
This work[a]	2.28 ± 0.05	4.49 ± 0.19	6.23 ± 0.23	7.83 ± 0.19	9.18 ± 0.26	10.44 ± 0.17

[a] Numerical fits.

Kawaler & Weiss (1991) have obtained the values of λ_i which, for comparison purposes (see later), we have reproduced in Table 1. Note the relatively small values of the rms deviations. Their results suggest that a semianalytic approach based on equation (17) can be quite useful for discussing the spectrum of trapped modes in a white dwarf.

In order to test this approach further, we have considered a large number of models taken from the extensive pulsation survey carried out by Brassard et al. (1991d). This adiabatic survey is based on the ZZ Ceti evolutionary calculations of Tassoul et al. (1990), and provides periods, kinetic energies, and first-order rotation coefficients C_{kl} for all g-modes with $l = 1$, 2, and 3 and periods less than or equal to 1000 s. Using the periods of trapped modes in the outer hydrogen layer (identified by primary minima in kinetic energy and/or maxima in C_{kl}), we have computed the first six trapping coefficients λ_i in conjunction with equation (17). Our results are summarized in the last row of Table 1. These numbers represent *average values* of the trapping coefficients for a very large number of trapped modes identified in ZZ Ceti models with masses in the range 0.4–0.8 $M_\odot$, effective temperatures in the range 15,000 K $\gtrsim T_{\rm eff} \gtrsim$ 10,000 K, and hydrogen layer masses in the range $-4 \gtrsim \log q({\rm H}) \gtrsim -14$. As can be inferred from the relatively small values of the rms deviations and in agreement with Kawaler & Weiss (1991), we find that the trapping coefficients are quite insensitive to these model parameters. Furthermore, our results are remarkably similar to those of Kawaler & Weiss (1991), indicating the excellent consistency between the two independent sets of calculations.

However, we have also found that the trapping coefficients do depend in a systematic way on the convective efficiency used in the construction of the ZZ Ceti star models. The coefficients listed in Table 1 refer to ML1 convection in the notation of Tassoul et al. (1990). For the relatively small convective efficiency of the ML1 treatment, the outer hydrogen convection zone remains thin enough for $T_{\rm eff} \gtrsim$ 11,000 K that the pulsation periods and the trapping coefficients are not affected. For a higher convective efficiency, however, the convection zone starts to overlap somewhat with the region of period formation in the range of effective temperatures of interest for the ZZ Ceti stars. For instance, using many additional models computed with efficient ML3 convection, we have calculated another set of trapping coefficients which show a sensitivity to effective temperature. Table 2 gives the ratios $\lambda_i({\rm ML3})/\lambda_i({\rm ML1})$ of the average trapping coefficients obtained for the two convective efficiencies considered here as a function of effective temperature. At $T_{\rm eff}$ = 13,500 K, there is practically no difference in the depth of the hydrogen convection zone computed with either ML1 or ML3 convection (see, e.g., Fig. 9 of Tassoul et al. 1990), so that the eigenfunctions of the two kinds of models are equally affected by convection, which leads to the same period spectrum and the same trapping characteristics. At lower effective temperatures, the base of the hydrogen convection zone sinks deeper in the star for ML3 models as compared with ML1 models, and the pulsation eigenfunctions are more perturbed by the presence of convection, which, ultimately, changes the periods of all modes (including trapped modes). Table 2 shows that this differential effect is larger for smaller effective temperatures (at least in the range shown), and is also larger for the higher order trapped modes. In particular, we can observe that the *period spacings* between trapped modes are *larger* for the ML3 models. This is one characteristic which may eventually be used to calibrate the mixing-length theory in real ZZ Ceti pulsators.

Before proceeding, it is interesting to point out that a surprisingly accurate *independent* estimate (i.e., not based on numerical fits of detailed pulsation calculations) can be obtained for λ_1, the first trapping coefficient. Indeed, in the Cowling approximation, the Cox-Saio boundary condition (Saio & Cox 1980) at the surface of a pulsating star may be written

$$y_1 = \frac{1 - [l(l+1)]/(C_1\omega^2 V)}{1 - (4 + C_1\omega^2)/V}\, y_2 , \qquad (18)$$

where $C_1 = (r/R)^3 M/M(r)$ (not to be confused with the previous C_1 encountered above), and the other symbols have been defined previously. At the surface of a star $C_1 = 1$, and for conditions appropriate to the outer layers of a white dwarf, $\omega^{-2} \gg 1$ and $V \gg 1$. This implies that

$$y_1 \simeq \left[1 - \frac{l(l+1)}{\omega^2 V}\right] y_2 . \qquad (19)$$

Hence, the first node of y_1 (counted from the surface) reaches that surface from below and eventually pops out of the star when the frequency of the g-mode becomes equal to and

TABLE 2

EFFECTS OF ML3/ML1 CONVECTION ON TRAPPING COEFFICIENTS

$T_{\rm eff}$ (K)	λ_i (ML3)/λ_i (ML1)					
	$i = 1$	$i = 2$	$i = 3$	$i = 4$	$i = 5$	$i = 6$
13,500	1.000	1.000	1.000	1.000	1.000	1.000
13,000	0.987	0.996	1.005	1.008	1.016	1.035
12,500	0.969	0.985	1.006	1.047	1.080	1.135
12,000	0.962	0.976	1.012	1.074	1.108	1.167
11,500	0.959	0.972	1.030	1.088	1.129	1.176
11,000	0.959	0.970	1.049	1.105	1.131	1.184

smaller than a critical frequency given by

$$\omega_c = \left[\frac{l(l+1)}{V}\right]^{1/2}, \tag{20}$$

which is the same (to within a factor of $\Gamma_1^{1/2}$) as one derived by Hansen, Kawaler, & Winget (1985) using other methods. This effect arises in a model because the pressure at the surface of the model is not strictly zero. Physically, this critical frequency corresponds (within a factor of $\Gamma_1^{1/2}$) to the frequency below which the condition of pure reflection is not expected to be valid for g-modes and is analogous to the critical Lamb frequency for pressure modes. Because the condition $y_1 = 0$ just above the H/He interface is also a condition for mode trapping (see previous discussion and following section), we can use equation (20) there to estimate the period of the first trapped mode. In other words, we now place the "surface" of the star at various depths corresponding to the different locations of the H/He interface in various models. This will be valid as long as the conditions under which equation (20) has been derived are fulfilled. These conditions are respected if $(1 - r/R) \ll 1$ and $[1 - M(r)/M] \ll 1$, which is indeed largely satisfied in the outer envelope of a white dwarf. Equation (20) can be rewritten to give an estimate of the period of the first trapped mode,

$$P_{1l} = 2\pi \Big/ \left[\frac{l(l+1)}{V}\frac{GM}{R^3}\right]^{1/2}. \tag{21}$$

If we combine this with equation (17), we find

$$\lambda_1 = \left[\left(1 - \frac{r_H}{R}\right)V\right]^{1/2}. \tag{22}$$

The first advantage of equations (21) and (22) is that they allow us to estimate P_{1l} and λ_1 solely on the basis of the properties of the equilibrium models, without doing any pulsation calculations. We find it remarkable that global properties such as P_{il} and λ_i can be estimated from local quantities. We have computed these quantities directly from equations (21) and (22) in a series of 0.6 $M_\odot$, ~12,500 K, ML1 ZZ Ceti star models with the same helium layer mass [$\log q(\mathrm{He}) = -2.0$] and for varying hydrogen layer masses in the range $-6 \geq \log q(\mathrm{H}) \geq -14$. Column (1) of Table 3 identifies the evolutionary sequence in the notation of Tassoul et al. (1990). Column (2) gives the effective temperature of the particular model selected. Columns (3) and (4) give, respectively, the "reduced" period $\tilde{P}_{1l} = P_{1l}[l(l+1)]^{1/2}$ as given by equation (21) and as obtained from the exact numerical results (averaged over $l = 1$, 2, and 3). Column (5) gives the relative error. Likewise, columns (6)–(8) give λ_1(model) as derived from equation (22), λ_1(pulsation) obtained from the exact numerical calculations (again averaged over $l = 1$, 2, and 3), and the relative error, respectively. To obtain $\tilde{P}_{1l}$(model) and λ_1(model), the H/He "interface" was defined in all models as the location where the helium fractional mass $Y = 0.5$. We find that the agreements between $\tilde{P}_{1l}$(model) and $\tilde{P}_{1l}$(pulsation) as well as between λ_1(model) and λ_1(pulsation) are excellent, given the very simple analytic approach used here to compute the "model" quantities.

The second advantage of our prescription (eq. [22]) is that the observed insensitivity of λ_1 to changes in model parameters is explained naturally here. Indeed, because $r \simeq R$ and $M(r) \simeq M$, $1 - r_H/R \equiv \Delta r/R \ll 1$, and we can write, approximately,

$$\left(1 - \frac{r_H}{R}\right)V \simeq \frac{\Delta r}{R}\frac{GM}{R}\frac{\rho}{P} = \frac{\rho g \Delta r}{P}. \tag{23}$$

However, from the equation of hydrostatic equilibrium, we can write the pressure at the H/He interface as

$$P \simeq \rho g \Delta r, \tag{24}$$

to within a factor of order unity. This means that $\lambda_1 \simeq$ constant of order unity, *independent* of the mass of the model, the effective temperature, and the location of the H/He interface.

We now transform the functional dependence of our central result (eq. [17]) to render it more useful from the point of view of interpreting the observations. Some guidance can first be gathered by using simple analytic envelope models. For example, it is well known that the pressure and the temperature of a thin stellar envelope assumed to be purely radiative and with an opacity given by a Kramers law are related by

$$P^2 \propto \frac{M}{R^2 T_{\mathrm{eff}}^4} T^{8.5}. \tag{25}$$

TABLE 3

COMPARISON OF PERIOD AND TRAPPING COEFFICIENT OF FIRST TRAPPED MODE[a]

Sequence (1)	T_{eff} (K) (2)	$\tilde{P}_{1l}$(model) (3)	$\tilde{P}_{1l}$(pulsation) (4)	% Error (5)	λ_1(model) (6)	λ_1(pulsation) (7)	% Error (8)
60206C1	12275	279.4	287.7	−2.9	2.20	2.27	−3.1
60207L1	12332	364.4	375.5	−3.0	2.27	2.34	−3.0
60208L1	12491	466.7	472.0	−1.1	2.29	2.32	−1.3
60209L1	12364	617.5	608.6	1.5	2.38	2.34	1.7
60210L1	12518	788.3	780.9	0.9	2.39	2.37	0.8
60212L1	12524	1263.2	1214.4	4.0	2.36	2.27	4.0
60213L1	12535	1547.3	1552.6	−0.3	2.25	2.25	0.0
60214L1	12149	1868.3	1945.0	−3.9	2.02	2.10	−3.8

[a] As obtained from detailed pulsation calculations and from model properties in representative cases.

Assuming further that hydrogen is completely ionized and that it forms an ideal, nondegenerate gas ($P \propto \rho T$), it is possible to integrate the mechanical structure equations (dP/dr and dM/dr) to obtain

$$\left(1 - \frac{r_H}{R}\right) \propto q(\mathrm{H})^{0.24} T_{\mathrm{eff}}^{0.48} R^{0.30} M^{-0.65}, \quad (26)$$

where $q(\mathrm{H})$ is the fractional mass of the hydrogen layer. Combining with equation (17) and an appropriate mass-radius relationship for the masses of interest ($M \propto R^{-1.53}$), we find

$$P_{il} \propto q(\mathrm{H})^{-0.12} M^{-1.06} T_{\mathrm{eff}}^{-0.24}. \quad (27)$$

Guided by this result, we have sought similar power laws from the detailed pulsation results of Brassard et al. (1991d). We have considered a large number of models in this procedure and have obtained average values of the exponents. Our final result is

$$P_{il} = \frac{18.01}{[l(l+1)]^{1/2}} \times \frac{\lambda_i}{q(\mathrm{H})^{0.102} (M/M_\odot)^{1.079} (T_{\mathrm{eff}}/11{,}500)^{0.220+(i-1)0.021}} \mathrm{s}, \quad (28)$$

where the first six values of λ_i can be obtained from Tables 1 and 2, depending on the convective efficiency assumed (ML1 or ML3). The exponent of the effective temperature contains a slight sophistication to take into account the fact that the high-order modes are more sensitive to a change in effective temperature. Extensive comparison with the exact numerical results indicates that equation (28) reproduces the periods of trapped modes to better than a few percent for a wide range of values of $q(\mathrm{H})$, M, and T_{eff} of potential interest for ZZ Ceti stars. Part of Table 4 contrasts the exact periods of the trapped modes found in our reference model (col. [4]) with the periods computed from equation (28) (col. [5]) for $i \leq 6$. The errors given (col. [6]) are quite typical.

Given some reasonable estimates of the effective temperature and the mass of a ZZ Ceti star, and given that trapped modes have been identified (through characteristic period spacings and ratios; see § 6), formula (28) becomes most useful for estimating the hydrogen layer mass, $q(\mathrm{H})$, in the star. We believe that this quantity can be obtained to well within the order of magnitude. The preliminary results of Kawaler (1991) and Kawaler & Weiss (1991), based on a somewhat less sophisticated formula than our equation (28), have already shown tantalizing prospects for measuring $q(\mathrm{H})$ in several ZZ Ceti stars.

4. A MORE FORMAL APPROACH TO MODE TRAPPING THROUGH THE USE OF ASYMPTOTIC THEORY

Beyond the simple model developed in the previous section, it is highly desirable to study further the phenomenon of mode trapping in models of pulsating DA white dwarfs. In particular, it is of prime interest to investigate the effects of composition layering on the *full* period spectrum and not only on that of trapped modes as we have done above. Moreover, a purely analytic approach can nicely complement the results of detailed numerical calculations and render them more transparent. Thus, in this section, we present a more rigorous description of mode trapping through the use of asymptotic theory. The basic theoretical foundations of our approach have already been laid down in the comprehensive paper of Tassoul (1980). We use and adapt the detailed analytic solutions of the equations for nonradial pulsations presented in that paper.

The period spectrum of a ZZ Ceti star model is perturbed by the presence of discontinuities in the Brunt-Väisälä frequency profile caused by the change in chemical composition in both the H/He and He/C transition zones as well as the presence of a thin hydrogen convection zone in the outermost layers. As discussed in § 2, the composition transition zones introduce

TABLE 4

PREDICTED PERIODS FOR TRAPPED MODES IN REFERENCE MODEL

l (1)	i (2)	k (3)	Period (4)	Prediction (λ_i) (5)	% Error (6)	Prediction (χ^2) (7)	% Error (8)
1	1	7	550.32	517.9	5.89	554.17	0.70
1	2	16	1034.98	1018.0	1.64	1032.22	0.27
1	3	22	1367.73	1410.0	3.09	1370.72	0.22
2	1	6	311.31	299.0	3.96	306.52	1.54
2	2	15	587.96	587.7	0.04	582.53	0.92
2	3	21	779.46	814.0	4.43	777.96	0.19
2	4	28	998.31	1021.3	2.30	1000.24	0.19
2	5	35	1222.25	1195.2	2.21	1222.53	0.02
2	6	40	1388.05	1356.9	2.30	1391.11	0.22
3	1	6	223.52	211.4	5.42	226.24	1.21
3	2	15	421.62	415.6	1.43	421.40	0.05
3	3	21	557.67	575.6	3.22	559.59	0.34
3	4	27	696.05	722.2	3.76	697.78	0.25
3	5	34	853.98	845.2	1.03	854.97	0.12
3	6	40	990.88	959.5	3.17	993.16	0.23
3	7	46	1132.49	...	...	1131.35	0.10
3	8	53	1294.75	...	...	1288.53	0.48

spikes, whereas the convection zone produces a well in the N^2 distribution. Formally, it is therefore necessary to divide the star in several regions and match the various analytic solutions at the many interfaces. This rapidly becomes unmanageable. To keep matters as simple as possible, we consider, in what follows, that there is *only one* discontinuity in the N^2 distribution between the center and the surface of the star. We focus on the H/He interface, although the formalism is applicable to the other discontinuities as well. In particular, this applies to a convection zone, provided that the zone remains thin enough for the two propagation zones to remain coupled.

We idealize the situation further by assuming that the H/He transition zone can be considered as a *true* discontinuity. Indeed, we have first experimented with square barriers (and wells) to mimic a spike (or well) of finite width in the N^2 distribution. We quickly realized, however, that the specification of width in addition to strength and location complicates the mathematics significantly without adding much to the essential physics. Hence, we have done away with this complication. Physically, this is justified as long as the width of the H/He spike remains small compared with the extent of the region of period formation. This is always the case in our DA white dwarf models. Note that the *details* of the g-mode period distribution do depend on the actual shape of the H/He composition spike, but the *essential* features do not.

The equations describing nonradial adiabatic pulsations in the Cowling approximation used by Tassoul (1980, eqs. T[1] and T[2] [from now on, we use the nomenclature and equation numbers of that paper but preface those numbers by a "T"]) are written with ξ_r and P' as independent variables. At a discontinuity of unspecified nature, this may pose a potential problem because it is δP, the Lagrangian perturbation of the pressure, not P', which should be continuous (Schutz 1980). However, for a discontinuity in the Brunt-Väisälä frequency *only* (such as the one we wish to consider here), the condition for the continuity of δP at the interface reduces to the same expression as that for the continuity of P', and we may use directly the expressions of Tassoul (1980). In terms of her modified independent variables S_1 and S_2 (eqs. T[76] and T[77]), the conditions of continuity of the eigenfunctions y_1 and y_2 can be written as

$$S_1^+ = \alpha S_1^- \tag{29}$$

and

$$\alpha S_2^+ = S_2^- , \tag{30}$$

where $\alpha \equiv (N_+/N_-)^{1/2}$ and N_+ (N_-) is the Brunt-Väisälä frequency above (below) the discontinuity.

We can write asymptotic expressions valid in the two zones of interest in our model (i.e., above and below the discontinuity). Assuming a purely radiative model, the first-order asymptotic expressions for S_1 and S_2 can be written (from eq. T[82]) for $x\,(=r/R) \le 1$, near the surface,

$$S_1 \approx k_o v_o^{1/2} J_{n_e+1}\left(\frac{v_o}{\sigma}\right) \propto k_o \sin\left(\frac{v_o}{\sigma} - \frac{n_e\pi}{2} - \frac{\pi}{4}\right), \tag{31}$$

$$S_2 \approx -k_o v_o^{1/2} J_{n_e}\left(\frac{v_o}{\sigma}\right) \propto -k_o \cos\left(\frac{v_o}{\sigma} - \frac{n_e\pi}{2} - \frac{\pi}{4}\right), \tag{32}$$

where k_o is an arbitrary constant, n_e is the effective polytropic index of the surface zone, σ is, as before, the eigenfrequency, and v_o is given by (eq. T[81])

$$v_o = [l(l+1)]^{1/2} \int_x^1 \frac{|N|}{x}\, dx , \tag{33}$$

where N is the Brunt-Väisälä frequency. In equations (31) and (32), we have used the asymptotic expressions for the Bessel functions for large values of the arguments.

In the core region, for $x \ge 0$, we have, from equation T(79),

$$S_1 \approx k_i v_i^{1/2} J_{l+1/2}\left(\frac{v_i}{\sigma}\right) \propto k_i \sin\left(\frac{v_i}{\sigma} - \frac{l\pi}{2}\right), \tag{34}$$

$$S_2 \approx -k_i v_i^{1/2} J_{l+3/2}\left(\frac{v_i}{\sigma}\right) \propto k_i \cos\left(\frac{v_i}{\sigma} - \frac{l\pi}{2}\right), \tag{35}$$

where k_i is an arbitrary constant, and v_i, defined by equation T(78), is

$$v_i = [l(l+1)]^{1/2} \int_0^x \frac{|N|}{x}\, dx . \tag{36}$$

Matching expressions (31) and (32) and (34) and (35) at the discontinuity, using conditions (29) and (30), we get, after some algebra, a transcendental equation of the form

$$\cot\left[\left(\frac{2P}{\Pi_{\mathrm{H},l}} - \frac{2P}{\Pi_{0,l}} + l\right)\frac{\pi}{2}\right] = \alpha^2 \cot\left[\left(\frac{2P}{\Pi_{\mathrm{H},l}} - n_e - \frac{1}{2}\right)\frac{\pi}{2}\right], \tag{37}$$

and the condition

$$k_i^2 = \frac{k_o^2}{\alpha^2}\left[\alpha^4 \cos^2\left(\frac{P\pi}{\Pi_{\mathrm{H},l}} - \frac{n_e\pi}{2} - \frac{\pi}{4}\right) + \sin^2\left(\frac{P\pi}{\Pi_{\mathrm{H},l}} - \frac{n_e\pi}{2} - \frac{\pi}{4}\right)\right]. \tag{38}$$

In the last two equations, P is the period and $\Pi_{0,l}$ is defined by

$$\Pi_{0,l} = \frac{\Pi_0}{[l(l+1)]^{1/2}} \equiv \frac{2\pi^2}{[l(l+1)]^{1/2}} \Big/ \int_0^1 \frac{|N|}{x}\, dx , \tag{39}$$

where Π_0 is a characteristic period of the star and corresponds to the usual period spacing as defined in Kawaler (1986), for example. Also,

$$\Pi_{\mathrm{H},l} = \frac{\Pi_{\mathrm{H}}}{[l(l+1)]^{1/2}} \equiv \frac{2\pi^2}{[l(l+1)]^{1/2}} \Big/ \int_d^1 \frac{|N|}{x}\, dx , \tag{40}$$

where d is the value of x at the discontinuity and Π_{H} is a characteristic period associated with the trapping region, which, in our specific case of interest, is the hydrogen layer. We note that our approach is very similar to that used by Berthomieu & Provost (1988) in a slightly different context (compare, e.g., their eq. [1] with our eq. [37]).

Equation (37) is a very important result of the present section. It gives, in the asymptotic limit of high radial overtones, the *complete* g-mode period spectrum of a pulsating star containing a discontinuity in its Brunt-Väisälä frequency profile. The strength of the discontinuity is measured by the parameter α, and the location of the discontinuity, d, enters in the evaluation of the integral $\Pi_{H,l}$. In view of its importance, some details about solving equation (37) may be relevant. After specifying the parameters Π_0, Π_H, n_e, and α^2 (which characterize a model and its discontinuity) as well as the spherical harmonic index l of a sequence of modes, the periods P which satisfy equation (37) are found by searching the zeros of a discriminant function defined as the right-hand side minus the left-hand side of the equation. This search is made by dividing our period window in a fine mesh. We use a period step of $\Pi_{0,l}/1000$ to define our mesh. When we find a change of sign in the discriminant function between two mesh points, we look for a possible zero of this function between these two points and then try to converge to a single period value in the previously obtained interval by a simple bisection convergence algorithm. If the algorithm fails to converge to a zero value for the discriminant function, the associated period is rejected because, in that case, it corresponds to an asymptote. Repeating this procedure over all our period window produces the desired period spectrum. This gives good results for values of α^2 up to 10. For larger α^2 values, the basic period step must be lowered, for example to $\Pi_{0,l}/10{,}000$, because some modes are missed during the whole procedure.

As an illustrative example of the use of equation (37), we have calculated what could be called a "synthetic" period spectrum using the following parameters which are typical of pulsating DA white dwarf models (see below): $\Pi_0 = 80$ s, $\Pi_H = 500$ s, $n_e = 3.0$, and $\alpha^2 = 4.0$. The modes considered have $l = 3$. Figure 8 shows a plot of the resulting periods expressed in terms of the radial order for the first several modes. The format is identical to that of Figure 6, which is based on detailed numerical calculations carried out with our reference model (see § 2). Keeping in mind that the present results are valid for large values of k, we find that the similarity between the two figures is striking. The same comment can be made when comparing our synthetic ΔP versus P diagram (Fig. 9) with Figure 7, also based on detailed numerical calculations. Quite clearly, equation (37) reproduces successfully the essential features of the nonuniform period distribution of the detailed model. Note that three different cases are illustrated in Figure 9; $\alpha^2 = 2.0$ (*solid curve*), $\alpha^2 = 4.0$ (*dotted curve*), and $\alpha^2 = 8.0$ (*dashed curve*). These results show explicitly that, as expected, increasing the strength of the discontinuity (increasing α) increases the deviations from constant period spacing. In addition, we find that the interval between minima in ΔP corresponds to $\Pi_{H,3}$ (=144 s). *This demonstrates that the period spacing between trapped modes (those which occupy the minima in Fig. 9) depends directly on the location of the discontinuity and, therefore, on the thickness of the outer hydrogen layer.* From equation (40) we find that the thinner the hydrogen layer, the larger the period spacing between trapped modes—a result also contained in equation (17).

Additional interesting results can be obtained from a further analysis of equations (37) and (38). We specialize, in part of what follows, to the case of the period spectrum of trapped

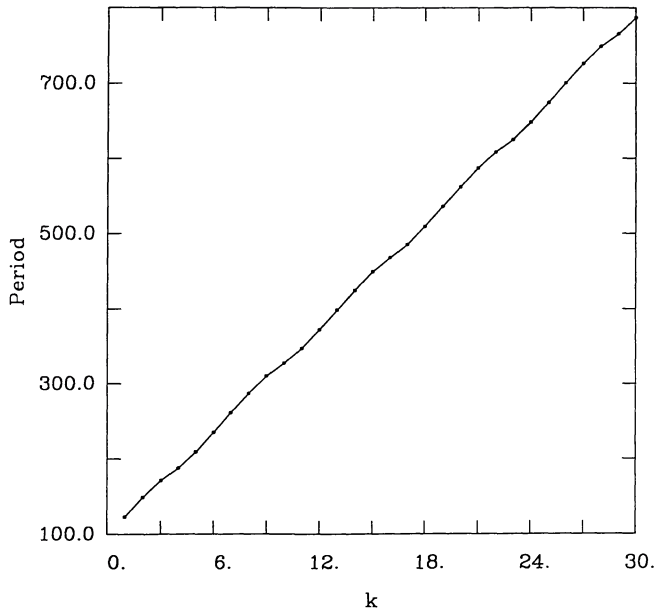

FIG. 8.—Synthetic period distribution (period vs. k) for $l = 3$ modes generated by our asymptotic model using $\Pi_0 = 80$ s, $\Pi_H = 500$ s, $n_e = 3.0$, and $\alpha^2 = 4.0$.

modes only. First, we can observe that, for the special case $\alpha = 1$ (no discontinuity in the Brunt-Väisälä frequency), equation (37) leads to an equality (within multiples of π) of the arguments of the two cotangents. This immediately leads to the *uniform* period spectrum of Tassoul (1980, eq. T[123]),

$$P = \left(2k + l + n_e + \frac{1}{2}\right)\frac{\Pi_{0,l}}{2}, \tag{41}$$

where k (=1, 2, . . .) is the radial order of the mode. Now, if we consider the opposite case, when the inner zone is completely or almost completely degenerate, the Brunt-Väisälä frequency is zero (or nearly so) there, and the wave cannot propagate in the core. The direct implication is that *all* the modes are trapped in the envelope, and the solution of equation (37) can be written when $\alpha \to \infty$ as

$$P = \left(2i + n_e - \frac{1}{2}\right)\frac{\Pi_{H,l}}{2}, \tag{42}$$

where i (=1, 2, . . .) is the number of nodes in the surface zone. Here we have used the fact that equation (37) can only be satisfied near a zero of the cotangents when $\alpha \to \infty$. The same solution (eq. [42]) would be obtained for the case of an isolated but *perfectly trapped mode* among the many modes of the spectrum. Indeed, such a mode would not propagate in the inner zone, and the structure of that zone cannot affect the value of the period. The result is thus independent of Π_0, and equation (42) must be again appropriate. Hence, we can consider equation (42) valid for *perfectly* trapped modes, and equation (41) valid when there is *no* trapping at all.

These two limiting cases immediately lead to a useful result for the (imperfectly) trapped modes of the kind encountered in ZZ Ceti star models. For instance, in a first approximation,

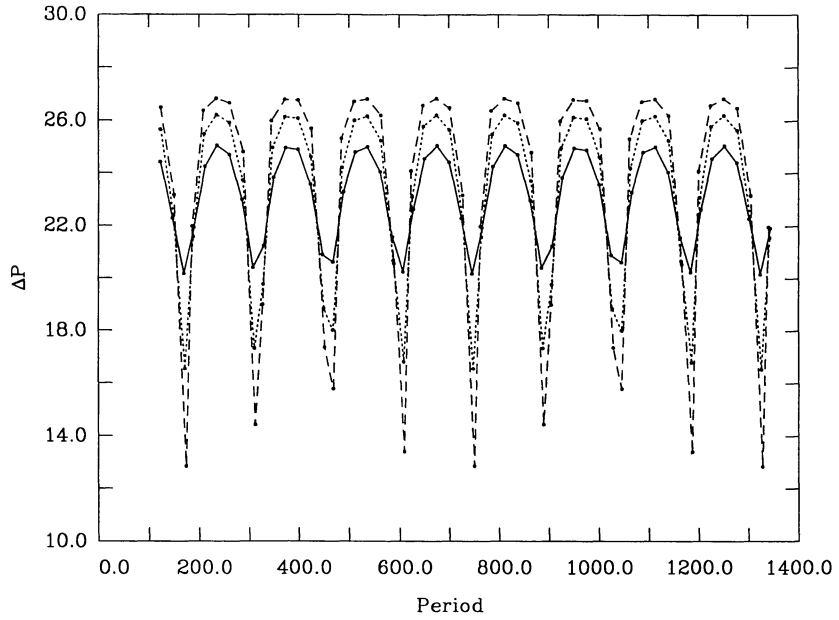

FIG. 9.—Synthetic period distribution (period spacing vs. period) for $l = 3$ modes generated by our asymptotic model using $\Pi_0 = 80$ s, $\Pi_H = 500$ s, $n_e = 3.0$, and $\alpha^2 = 2.0$ (*solid curve*), $\alpha^2 = 4.0$ (*dotted curve*), and $\alpha^2 = 8.0$ (*dashed curve*).

the period of such a trapped mode must be given by *both* equations (41) and (42). This implies that the period spacing between two consecutive trapped modes ($\Delta i = 1$) separated by an interval (Δk) in radial order is roughly given by

$$\Delta P \simeq \Delta k \Pi_{0,l} \simeq \Pi_{H,l} , \tag{43}$$

where equations (41) and (42) have been used. Hence, the interval Δk between two consecutive trapped modes is approximated by

$$\Delta k \simeq \frac{\Pi_H}{\Pi_0} . \tag{44}$$

This result will be used below.

As discussed previously, trapped modes also leave a distinct signature on the kinetic energy density profile across the discontinuity (see § 2 and Fig. 3). We can use this property to identify trapped modes in connection with equations (37) and (38). We first evaluate the mean kinetic energy between nodes of the eigenfunctions S_2 in the vicinity of the interface (i.e., above and below) as

$$\langle E_{kin} \rangle \propto \langle (P'/\rho)^2 \rangle \propto \langle N S_2^2 \rangle , \tag{45}$$

where we have used the definition of S_2 (eq. T[77]) and have neglected the amplitude variations between nodes, the variations of the gravitational potential (Cowling's approximation), and the radial contribution (y_1) to the kinetic energy. The ratio of the values of the kinetic energy below and above the discontinuity can be written (see eqs. [32] and [35])

$$\frac{\langle E_{kin} \rangle^-}{\langle E_{kin} \rangle^+} \approx \frac{N_- k_i^2}{N_+ k_o^2} = \frac{1}{\alpha^2} \frac{k_i^2}{k_o^2} = \frac{1}{\alpha^4} \left[\alpha^4 \cos^2 \left(\frac{P\pi}{\Pi_{H,l}} - \frac{n_e \pi}{2} - \frac{\pi}{4} \right) + \sin^2 \left(\frac{P\pi}{\Pi_{H,l}} - \frac{n_e \pi}{2} - \frac{\pi}{4} \right) \right] , \tag{46}$$

where the last equality comes from equation (38).

As we have seen above, modes which are trapped in the outer region above the H/He interface are characterized by the largest contrast in kinetic energy across the composition interface from the He- to the H-dominated side. Such modes must therefore show the *smallest* value of the ratio $\langle E_{kin} \rangle^- / \langle E_{kin} \rangle^+$. For $\alpha > 1$, the minimum value of this ratio is $1/\alpha^4$ and is obtained when

$$\cos \left(\frac{P\pi}{\Pi_{H,l}} - \frac{n_e \pi}{2} - \frac{\pi}{4} \right) = 0 . \tag{47}$$

This last relation implies that $S_2 = 0$ or, equivalently, $y_2 = 0$ at the interface. Noting that the expression $\alpha [= (N_+/N_-)^{1/2}] > 1$ corresponds to the *helium side* of the composition spike discontinuity in the Brunt-Väisälä frequency distribution of a realistic model, we recover our empirical condition for trapping: $y_2 \simeq 0$ at the interface, but *from below*. We note also that our estimate of a minimal value of $1/\alpha^4$ for the kinetic energy ratio can be made consistent with the observed contrast in energy

across the H/He interface for a trapped mode ($k = 6$) in our reference model (see Fig. 3) if we take $\alpha^2 \simeq 2$–3, a typical value for ZZ Ceti star models (see below).

It is also interesting to consider what happens on the hydrogen side of the composition transition zone spike. In that case, $\alpha < 1$, and the minimum value of the ratio $\langle E_{\rm kin}\rangle^-/\langle E_{\rm kin}\rangle^+$ is obtained by equating the sine-squared term in equation (46) to zero. This implies that $S_1 = 0$ or, equivalently, $y_1 = 0$ at the interface. Hence, we find a natural explanation for our second empirical observation that $y_1 \simeq 0$ at the interface, but *from above,* for modes which are trapped in the outer hydrogen layer. Note that the actual minimum value of the ratio $\langle E_{\rm kin}\rangle^-/\langle E_{\rm kin}\rangle^+$ is now equal to unity (i.e., there is no contrast in kinetic energy immediately above the interface), which simply reflects the fact that the behavior of the kinetic energy is (within our approximation) totally independent of the radial motions associated to y_1.

As an important aside, we may also point out that seeking the conditions which *maximize* the energy ratio in equation (46) would also lead to trapped modes, but those would correspond to trapping in the *interior* region below the H/He interface. At this point, in order to avoid confusion, we will retain the term "trapping" only for trapping in the outer hydrogen layer, while we will use the term "confinement" for modes which are (or tend to be) trapped below the composition transition zone. To obtain the optimum conditions for confinement, equation (46) suggests that y_1 should have a node just *below* the H/He transition zone, while y_2 should have its corresponding node just *above* the composition interface. However, this is not possible in the envelopes of white dwarfs where, as observed previously, a given node of y_1 is always above its corresponding node in y_2. Hence, confinement cannot lead to effects as dramatic as those caused by trapping. Nevertheless, composition layering leads to those two intimately related physical phenomena. For example, in Figure 2, modes which tend to be confined below the H/He interface are those corresponding to the *maxima* in total kinetic energy. It is important to realize that the kinetic energies of these confined modes are *larger* than the kinetic energies obtained for a chemically homogeneous model (see Brassard et al. 1991d). Because the optimum conditions for confinement are fulfilled to a lesser degree than for trapping, confinement leads to *broad* maxima in Figure 2, in contrast to the relatively *sharp* minima associated with trapping.

A further look at equation (47) indicates that it leads directly to a period spectrum given by equation (42), which corresponds to perfect trapping in the hydrogen layer. Likewise, equation (47) implies that *both* sides of equation (37) are individually equal to zero, which *cannot* be satisfied at the same time because of the integer values of k, i, and l and because Π_0 and $\Pi_{\rm H}$ are independent parameters. Thus, in practice, the conditions for maximum (perfect) trapping cannot be met, and equation (37) cannot be exactly equal to zero. In particular, when $y_2 \simeq 0$, y_1 is no longer negligible, as has been implicitly assumed in the derivation of equation (47).

To satisfy equation (37) while still seeking optimum conditions for trapping, we must use series expansions around zeros of the cotangents. Doing this and keeping only the first-order terms, we find that the *period spectrum of trapped modes* can be approximated by the useful formula

$$P = \frac{1}{[l(l+1)]^{1/2}}\left[k + i(\alpha^2 - 1) + \frac{l}{2} + \frac{n_e\alpha^2}{2} - \frac{\alpha^2}{4} + \frac{1}{2}\right] \times \frac{\Pi_0\Pi_{\rm H}}{\Pi_{\rm H} + (\alpha^2 - 1)\Pi_0}\,. \quad (48)$$

This relation can be considered as some kind of interpolation formula between the case of maximum envelope trapping ($\alpha \to \infty$; eq. [42]) and the case of minimal trapping ($\alpha = 1$; eq. [41]). We recall that k corresponds to the usual radial order of the mode, i is a new quantum number giving the order of the *trapped* mode (equivalently, the number of zeros in the H layer), and α is a measure of the strength of the discontinuity in the Brunt-Väisälä frequency. This discontinuity plays a key role in specifying the period structure of compositionally stratified white dwarf models. It turns out that the essential physics of envelope trapping in white dwarfs is contained in equation (48).

Additional insight can be gained by studying this equation further. For instance, equation (48) indicates that the period spacing between two consecutive trapped modes is given by

$$P_{i+1} - P_i = \frac{\Delta k + \alpha^2 - 1}{[l(l+1)]^{1/2}}\frac{\Pi_0\Pi_{\rm H}}{\Pi_{\rm H} + (\alpha^2 - 1)\Pi_0}\,. \quad (49)$$

Assuming that the *mean* value of Δk is given by equation (44), we find that $\overline{P_{i+1} - P_i} = \Pi_{{\rm H},l}$, as expected from relation (42). Using this, we also find that the mean period spacing between two consecutive modes is given by $\overline{P_{k+1} - P_k} = \overline{P_{i+1} - P_i}/\overline{\Delta k} = \Pi_{0,l}$ as expected from relation (41).

A lower limit for ΔP can be obtained, knowing that the minimal value of ΔP arises in the vicinity of trapped modes (see, for example, Fig. 7). For a given trapped mode, equation (48) gives its period and also a good guess (as long as $\Pi_0 \ll \Pi_{\rm H}$) for the period of the following one ($\Delta k = +1$) because this adjacent mode is very nearly trapped. But this guess will be an underestimate of the period because the ΔP associated with this particular mode will be slightly higher than the one associated with the trapped mode. From these considerations about equation (48), we can set

$$[l(l+1)]^{1/2}(\Delta P)_{\rm min} \geq \frac{\Pi_0\Pi_{\rm H}}{\Pi_{\rm H} + (\alpha^2 - 1)\Pi_0} \equiv \Pi_{\rm min}\,. \quad (50)$$

Similar considerations can bring us an upper limit for ΔP. We can derive an expression similar to equation (48), but this time for the most confined modes, if we assume that the values of the cotangent functions in equation (37) are near $\pm\infty$ instead of zero. We then obtain a relation for confined modes which will overestimate the period of the mode following the most confined mode, thus giving the needed upper limit,

$$[l(l+1)]^{1/2}(\Delta P)_{\rm max} \leq \frac{\alpha^2\Pi_0\Pi_{\rm H}}{\alpha^2\Pi_{\rm H} + \Pi_0(1 - \alpha^2)} \equiv \Pi_{\rm max}\,. \quad (51)$$

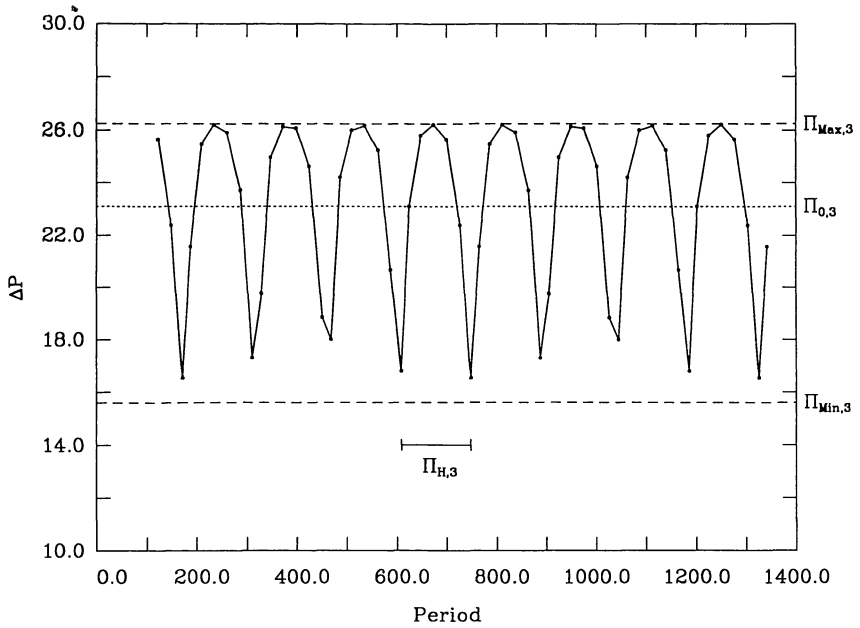

FIG. 10.—Same as Fig. 9, but only the results for the $\alpha^2 = 4.0$ model are shown (*solid line*). Also indicated are the minimum, maximum, and average period spacings of the distribution, as well as the cycle period between trapped modes.

Figure 10 reproduces the $\alpha^2 = 4.0$ curve of Figure 9, but this time we have included the lower (15.6 s), the mean (23.1 s), and the upper (26.2 s) limits on ΔP. The effects of the various parameters (Π_0, Π_H, n_e, and α^2) of equation (37) on the *entire* period structure can be seen in this last figure. First, Π_0 is the *mean* value of the period spacings between adjacent modes. It corresponds to the *constant* period spacing between adjacent modes obtained in the absence of discontinuity. Note that the period spacings between adjacent modes tend to be larger near confined modes, while they tend to be smaller near trapped modes as compared with the case with no discontinuity. Second, the curve of Figure 10 shows a quasi-periodic structure. As pointed out previously, the cycle period of this structure is given by Π_H and corresponds to the mean value of the period spacings between *trapped* (or confined) modes. The next parameter, n_e, can be interpreted as a phaselike parameter in our quasi-periodic curve, providing a starting value for $P(k = 1)$. Finally, again as pointed out before, α^2 is a measure of the departure of ΔP from Π_0, as can be seen by the values of Π_{min} and Π_{max}, which depend on α^2. Not unexpectedly, the agreement between the minimum ΔP values and the estimated lower limit given by equation (50) is worse than in the case of the maximum ΔP values and the upper limit given by equation (51). The reason here is that composition layering affects the period distribution to a higher degree in the vicinity of a trapped mode than in the neighborhood of a confined mode.

5. COMPARISON OF THE PREDICTIONS OF ASYMPTOTIC THEORY AND THE EXACT NUMERICAL RESULTS

In the last section, we found that the *entire* period structure of a stratified model (see eq. [37]) can be reproduced with four parameters: Π_0, Π_H, n_e, and α^2. We also found an expression (eq. [48]) giving the period spectrum of *trapped* modes using the same four parameters. Here we wish to examine more closely the question of how well (or how badly) these asymptotic expressions reproduce the g-mode periods obtained from detailed, exact numerical calculations. To this end, we first use a purely empirical approach which consists of obtaining the values of the four parameters which best fit the exact period distributions in our reference model and others. We will address the question of how to relate these empirically determined values of the parameters to the properties of the models themselves at the end of the section.

We begin with the period spectrum of the trapped modes of our reference model in the period window 0–1400 s for $l = 1, 2$, and 3. All together, there are 17 periods; these are given in column (4) of Table 4. An estimate of Π_H can be obtained from the mean period spacing between the trapped modes (see § 4). Using only modes with $i \geq 4$ (since our analytic model is strictly valid in the asymptotic limit of high radial overtones), we obtain $\Pi_H \simeq 504.8$ s. Likewise, an estimate of Π_0 is obtained from the relation $\Pi_0 \approx \Pi_H/\Delta k$ discussed previously. We thus obtain $\Pi_0 \simeq 79.69$ s. To get an idea of the accuracy of these figures, we can compare them with those obtained by considering only modes with $k \geq 70$, thus ensuring that the asymptotic regime is fully reached. This is possible from our especially computed reference model, for which we have periods up to 4000 s (these longer periods are not given in Table 4 but are available). In that case, we obtain $\Pi_H \simeq 550.8$ s and $\Pi_0 \simeq 80.95$ s. The 1.6% difference for Π_0 can readily be explained by the fact that, even with modes with $i \geq 4$, departures from the asymptotic regime cannot be totally neglected. The 9% difference for Π_H is more significant but can likewise be explained in terms of departures from the asymptotic behavior. Clearly, however, Π_H is a more sensitive quantity than Π_0, and this will be further discussed below.

The evaluation of the parameters n_e and α^2 from the period spectrum of trapped modes is less straightforward. We combine equations (48) and (50) to obtain an expression for the

periods which depends on three quantities (n_e, α^2, Π_{min}) which we treat as free parameters in a three-dimensional χ^2 fit. Knowing the periods and the indices l, i, and k of the 17 modes given in Table 4, we minimize in a χ^2 sense the global error (defined as the sum of the squares of the relative errors between the exact and predicted periods). To do this, we use the "downhill simplex" method of minimization as described in Press et al. (1986). The resulting best fit gives $n_e = 2.82$, $\alpha^2 = 2.27$, and $\Pi_{min} = 65.80$ s. The "predicted" periods obtained with these parameters are given in the column (7) of Table 4; the relative errors with respect to the exact periods are listed in the last column of the table. We note that the agreement is excellent. In particular, there is a significant increase in the accuracy achieved as compared with the results of our simple semianalytic formula for the periods of trapped modes (cols. [5] and [6] in Table 4). (In this connection, it is appropriate to point out that, contrary to superficial appearance, the results of the asymptotic theory developed in the previous section can, under certain additional approximations, be cast in the form of our semianalytic formula [see Appendix A].) Moreover, we also find an excellent degree of internal consistency in the sense that combining our independently estimated values of Π_H (504.8 s) and Π_0 (79.69 s) with our fitted value of α^2 (2.27) leads (via eq. [50]) to $\Pi_{min} \simeq 66.40$ s, a result consistent within 1% with the value Π_{min} (65.80 s) obtained in the χ^2 fit.

We have found it interesting and instructive to investigate how our fitting technique would perform along an evolutionary sequence of models (rather than for the case of only a single isolated model, considered up to now). To accomplish this, we have considered 10 additional models taken from the same 60210L1 sequence as our reference model. We have calculated the g-mode period spectra of these models in a period window (0–2000 s; $l = 1$, 2, and 3) half as wide as that of our reference model, and 500 quadratic elements were used. Otherwise, the periods are computed under the same assumptions (in particular, $B = 0$ in the He/C transition zone) as in the case of the reference model. In a way identical to that case, Π_H and Π_0 were estimated from the average period spacing and Δk between trapped modes, and n_e, α^2, and Π_{min} were obtained from a three-dimensional χ^2 fit. As before, only the periods of trapped modes with $i \geq 4$ were considered in this exercise. The results are summarized in Table 5. Column (1) gives the effective temperature of the evolving model, and columns (2)–(6) give, respectively, the derived values of Π_0, Π_H, n_e, α^2, and Π_{min} (the latter obtained from the χ^2 fit). Column (7) gives Π_{min} obtained from Π_0, Π_H, and α^2.

TABLE 5

PARAMETER VALUES OBTAINED FROM TRAPPED-MODE PERIOD SPECTRA OF AN EVOLUTIONARY SEQUENCE OF MODELS

T_{eff} (K) (1)	Π_0 (2)	Π_H (3)	n_e (4)	α^2 (5)	Π_{min}(fit) (6)	Π_{min} (7)
15587	69.75	476.6	3.38	1.50	65.16	65.00
14807	71.64	465.7	2.89	2.05	62.45	61.88
13969	73.47	489.8	3.51	1.56	68.10	69.61
13239	75.45	490.4	3.72	1.31	72.53	72.02
12518	79.69	504.8	2.82	2.27	65.80	66.40
11833	80.66	497.4	3.23	1.66	73.35	72.86
11377	81.80	531.7	3.07	1.78	73.84	73.04
11134	83.43	542.3	2.70	2.13	71.73	71.07
10925	85.45	569.6	1.95	4.47	56.68	56.20
10568	88.28	618.0	1.69	5.48	53.66	53.83
9999	91.44	658.3	1.42	6.66	51.21	51.19

The results shown in Table 5 are, at the same time, both gratifying and somewhat disappointing. First, as in the case of the reference model, we recover, for all models, the exact periods of the trapped modes to a high level of accuracy (typically, well below 1%) when the listed parameters [n_e, α^2, Π_{min}(fit)] are used in conjunction with our asymptotic formula (48). Moreover, the fitted values of Π_{min} agree closely with the derived values in all cases. Our mild disappointment comes from the behavior of some of the parameters as the evolution proceeds. For instance, we expect that both Π_0 and Π_H should increase monotonically with decreasing effective temperature along an evolutionary sequence (see Tassoul et al. 1990). Table 5 shows that this is indeed the case for Π_0, and (except for two cases) the same is true for Π_H. The two exceptional cases are inconsequential and simply reflect the lesser accuracy with which Π_H is obtained from period spacings as compared with Π_0. On the other hand, α^2 measures the strength of the discontinuity in the Brunt-Väisälä frequency and is directly related to the term B in equation (1). As shown by Tassoul et al. (1990), the B spike evolves extremely slowly in a ZZ Ceti star model, and this should be reflected by an essentially constant value of α^2 (particularly in the relatively narrow range of effective temperature considered in Table 5). Instead, α^2 shows substantial variations with effective temperature. However, we do observe that α^2 correlates negatively and strongly with n_e; when α^2 is large, n_e is small, and vice versa. This is an obvious hint that α^2 and n_e are coupled and cannot be considered as truly independent parameters *from the point of view of our equation (48)*. We can say that our three-dimensional χ^2 technique is quite successful at reproducing the periods of trapped modes, but that it fails, by itself, to provide independent and reliable values of α^2 and n_e. In this context, it is legitimate to suspect strongly that various couples [α^2, n_e] give rise to predicted periods of *comparable* accuracy, while the numerical technique simply picks up the *best* absolute fit. We need some external constraints on either one of these parameters to derive the most physically acceptable couple [α^2, n_e]; this is provided below.

Before considering these external constraints, however, we first demonstrate formally the existence of a coupling between α^2 and n_e, which is directly related to the particular functional form of equation (48). We show, through algebraic manipulations, that we can transform equation (48) to a form involving a couple [α^2, n_e]′ different from the "best" couple [α^2, n_e]. For instance, if we disregard the integer nature of the k-index (which is appropriate for large values of k), the quantum numbers of trapped modes are approximately related by

$$k \simeq k_o + i\Delta k - \frac{l}{2}, \tag{52}$$

where k_o is a reference number (which can be derived from the actual period spectrum for trapped modes), and Δk is the average spacing between two consecutive trapped modes. The term $l/2$ reflects the fact that, for a given i, the value of k changes by 1 when the value of l changes by 2 (see cols. (1)–(3) of Table

4). If we further assume that Δk is given by equation (44), we can rewrite equation (48) as

$$P \approx \frac{1}{[l(l+1)]^{1/2}}\left[k + \frac{l}{2} + \left(k_o + \frac{n_e\alpha^2}{2} - \frac{\alpha^2}{4} + \frac{1}{2}\right) \times \frac{\Pi_H}{\Pi_H + (\alpha^2 - 1)\Pi_0} - k_o\right]\Pi_0 , \quad (53)$$

where we have replaced i by its approximate value given by equation (52). With the definition

$$\frac{n'_e}{2} \equiv \left(k_o + \frac{n_e\alpha^2}{2} - \frac{\alpha^2}{4} + \frac{1}{2}\right) \times \frac{\Pi_H}{\Pi_H + (\alpha^2 - 1)\Pi_0} - k_o - \frac{1}{4} , \quad (54)$$

we finally obtain

$$P \approx \frac{1}{[l(l+1)]^{1/2}}\left(k + \frac{l}{2} + \frac{n'_e}{2} + \frac{1}{4}\right)\Pi_0 . \quad (55)$$

This last relation is equivalent to our formula (48), but this time written with the parameters α^2 and n_e equal to 1 and n'_e, respectively. Strictly speaking, the transformation which leads to equation (55) gives rise to a period spectrum for trapped modes which is *less* accurate than that provided by equation (48) because additional approximations have been made during the transformation. In practice, however, these approximations are fairly good, and the differences in the predicted periods given by equations (48) and (55) are reasonably small. Hence, we find that the accuracy of the predicted periods is only somewhat worsened when the best couple $[\alpha^2, n_e]$ is replaced by $[1, n'_e]$. Despite the rough equivalence from the point of view of the computed periods, the later choice of the parameters is clearly unphysical because $\alpha^2 = 1$ corresponds to the case where there is *no* discontinuity in the Brunt-Väisälä frequency, contrary to our basic premise.

The coupling between α^2 and n_e in equation (48) can also be studied from another angle. Figure 11 shows contour plots of the χ^2 values as functions of α^2 and n_e for our reference model. The value of χ^2 increases by a factor of 1.5 between successive contours. The small cross gives the position ($\alpha^2 = 2.27$, $n_e = 2.82$) of the absolute minimum in the χ^2 surface, which corresponds to the best fit to the period spectrum for that particular model as discussed above. What is striking in this plot, however, is the elongated "valley" (whose bottom is delineated by the dashed curve) in the χ^2 surface, which clearly reveals the coupling between α^2 and n_e. The bottom of the valley is fairly flat, which means that acceptable values of $[\alpha^2, n_e]$ (again, from the point of view of eq. [48]) can be found in a relatively wide range. For example, the transformation we just discussed would give $\alpha^2 = 1$ and $n_e (= n'_e) = 4.62$ for our reference model, just on the dashed line shown in the figure. Clearly, from the contour plots, these values would lead to an inferior χ^2 fit for the periods, but the accuracy remains acceptable in the present context. We note also that the values of $[\alpha^2, n_e]$ which give the best absolute fits to the period spectra of the other evolutionary

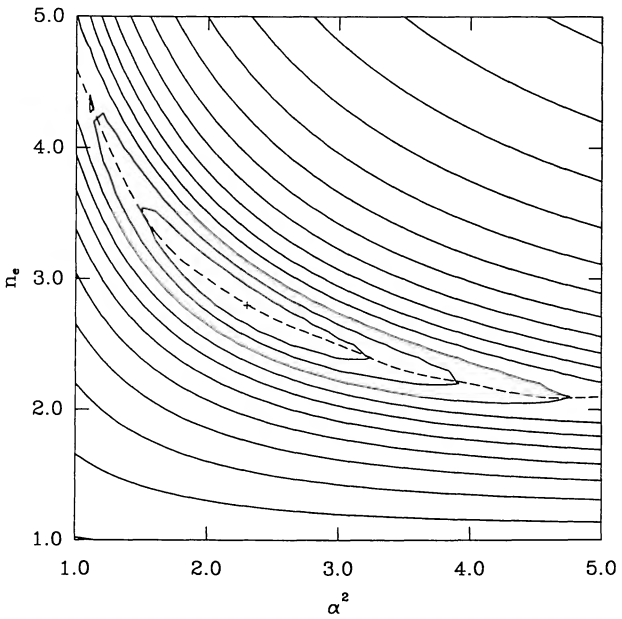

FIG. 11.—Contour plots of χ^2 values in the $[\alpha^2, n_e]$ plane for our reference model. The diagram shows a "valley" whose bottom is delineated by the dashed curve. Consecutive contour lines differ by a factor of 1.5 in their χ^2 values. The cross shows the absolute maximum depth of the valley.

models (see Table 5) all lie along the bottom of the valley in Figure 11. Given the inherent and unavoidable noise in the construction of realistic stellar models, and given the coupling between α^2 and n_e which characterizes equation (48), there thus should be no surprise that the couple $[\alpha^2, n_e]$ is somewhat "noisy" along the evolutionary sequence shown in Table 5. We conclude that, from the period spectrum of trapped modes *only*, our asymptotic theory cannot give us *independent* and accurate estimates of the parameters α^2 and n_e.

If we now consider the *full* period structure (instead of that of trapped modes only), we can hope that the additional information available will help to constrain these parameters better. And indeed, an estimate of α^2 can be obtained from the average of the *minimum period spacings between adjacent modes* (i.e., those found near trapped modes) in conjunction with equation (50). We note that α^2 could equally be estimated from maximum period spacings found near confined modes (see eq. [51]). However, as can be observed in Figure 7, the latter are more sensitive to residual structure than the former and, as such, are less useful in deriving α^2. Figure 7 also shows that the first several values of $(\Delta P)_{\min}$ (particularly those associated with the first trapped modes) are significantly smaller than the values obtained for the higher order modes. In order to avoid this regime where the asymptotic approximation fails and where the local wavelengths of the modes are much larger than the thickness of the composition transition zone, we have obtained, for each evolutionary model, the value $\bar{\Pi}_{\min}$ by averaging the $(\Delta P)_{\min}$ for all modes with $l = 1$, 2, and 3 and periods up to 2000 s, but for $i \geq 4$. The results are reported in column (4) of Table 6. Because the complete period spectrum obviously contains the period spectrum of the trapped modes, we have also reported the values of Π_0 and Π_H previously obtained from period spacings between trapped modes. Combining

TABLE 6

PARAMETER VALUES OBTAINED FROM FULL PERIOD SPECTRA

$T_{\rm eff}$ (K) (1)	Π_0 (2)	Π_H (3)	$\bar{\Pi}_{\rm min}$ (4)	α^2 (5)	$n_e(\alpha^2 = 2.28)$ (6)	$\Pi_{\rm min}(\alpha^2 = 2.28)$ (7)
15587	69.75	476.6	58.82	2.27	2.69	59.54
14807	71.64	465.7	60.37	2.21	2.74	60.83
13969	73.47	489.8	62.34	2.19	2.83	62.49
13239	75.45	490.4	63.46	2.23	2.72	64.27
12518	79.69	504.8	66.39	2.27	2.83	65.68
11833	80.66	497.4	67.19	2.24	2.73	67.77
11377	81.80	531.7	67.49	2.38	2.70	69.35
11134	83.43	542.3	70.13	2.23	2.61	70.41
10925	85.45	569.6	71.37	2.31	2.66	71.39
10568	88.28	618.0	73.43	2.42	2.63	73.22
9999	91.44	658.3	76.60	2.38	2.41	76.51

these three quantities according to equation (50), we obtain an estimate for α^2 listed in column (5) of the table. There is perhaps a slight hint that α^2 increases somewhat with decreasing effective temperature: $\bar{\alpha}^2 = 2.23 \pm 0.04$ for the five hotter models, while $\bar{\alpha}^2 = 2.37 \pm 0.07$ for the five cooler ones. However, this trend, if any, may not be significant, and we simply adopt here a mean value $\bar{\alpha}^2 = 2.28 \pm 0.08$ for the 11 models. This is now consistent with the expected slow evolution of the B spike alluded to above.

To test the internal consistency of our approach, we now go back to our central formula (eq. [48]) for the periods of trapped modes, but this time α^2 is fixed. We again fit equation (48) to the exact periods of trapped modes in a χ^2 sense, but we now have to deal with the simpler situation of a two-dimensional fit, n_e and $\Pi_{\rm min}$ being the independent parameters. Assuming that $\alpha^2 = 2.28$ as above, we obtain the values of n_e and $\Pi_{\rm min}$ given in columns (6) and (7) of Table 6. We find that the effective polytropic index, n_e, is fairly constant, with perhaps a slight tendency to decrease with decreasing temperature. In addition, and contrary to the situation illustrated in Table 5, we now recover the expected monotonic behavior of $\Pi_{\rm min}$ with effective temperature. Note, in particular, the excellent agreement between $\bar{\Pi}_{\rm min}$ obtained from averaging values of $(\Delta P)_{\rm min}$ and $\Pi_{\rm min}$ derived from the two-dimensional χ^2 fit.

The periods of trapped modes for our evolutionary models can now be reestimated by using our asymptotic relation (48), equation (50), and the values of α^2 (=2.28), n_e, and $\Pi_{\rm min}$ given in Table 6. We find that the accuracy of these new estimates as compared with the exact periods is only very slightly inferior to values derived from the corresponding parameters given in Table 5, and it is still, typically, well below 1%. For example, the average error for the periods of the first 17 trapped modes in our reference model is now 0.41%, comparable to the average error reported in Table 4. In fact, our new estimates of the periods of trapped modes based on the parameters of Table 6 are so close to periods given in Table 4 that it is not worth writing yet another comparison table.[2] The important difference here is that *independent* estimates of α^2 and n_e are now available. To achieve this, however, we recall that we had to use the additional information contained in the full period spectrum (as opposed to the period spectrum of trapped modes) to constrain the couple $[\alpha^2, n_e]$.

At this point, it is of interest to verify how well the sets of parameters (Π_0, Π_H, n_e, and α^2) we just obtained can reproduce the *entire* period distributions of chemically stratified stellar models. From Table 6, we take $\alpha^2 = 2.28$ and $n_e = 2.83$, appropriate for the reference model. However, instead of taking Π_0 and Π_H from that table, we prefer to use the values previously obtained by considering only trapped modes with $k \geq 70$ in the reference model: $\Pi_0 \simeq 80.95$ s and $\Pi_H \simeq 550.8$ s. This has some importance here because our analytic approach is expected to give the best results in the asymptotic limit of high radial overtones. We need to take this precaution to obtain the best possible results in the sensitive ΔP versus P diagram.

Figure 12 contrasts the period distributions of the $l = 3$ modes of our reference model in a ΔP versus P diagram as given by the exact numerical calculations (*dotted line*) and as obtained by our asymptotic theory (*continuous line*). In the latter case, the period spectrum has been obtained by solving the transcendental equation (37), where use of the above values of the parameters Π_0, Π_H, n_e, and α^2 has been made. The format of the figure is identical to that of Figure 7, except that the period window extents to 3000 s, in the fully asymptotic regime. There are differences between the two curves which can readily be accounted for. First, as discussed briefly in a previous section, the minima are much more pronounced for the first several trapped modes in the exact calculations. This is mostly caused by the finite width of the composition transition zone in the model; modes with relatively low values of k have radial wavelengths larger than the thickness of the transition zone. Modes of that sort that are consecutive are more strongly affected (in a differential sense) by the pinching effect of the

[2] Note that the predicted periods based on the values of α^2, n_e, and $\Pi_{\rm min}$ given in either Table 5 or Table 6 are obtained by combining eqs. (48) and (50) and using χ^2 fits. If we were to use directly the asymptotic expression (48) with values of Π_0, Π_H, n_e, and α^2 (again obtained from either Table 5 or Table 6), the predicted periods would be somewhat less accurate (with a typical average error twice as large as that previously quoted), because in doing so we would forfeit the benefits of the χ^2 fits.

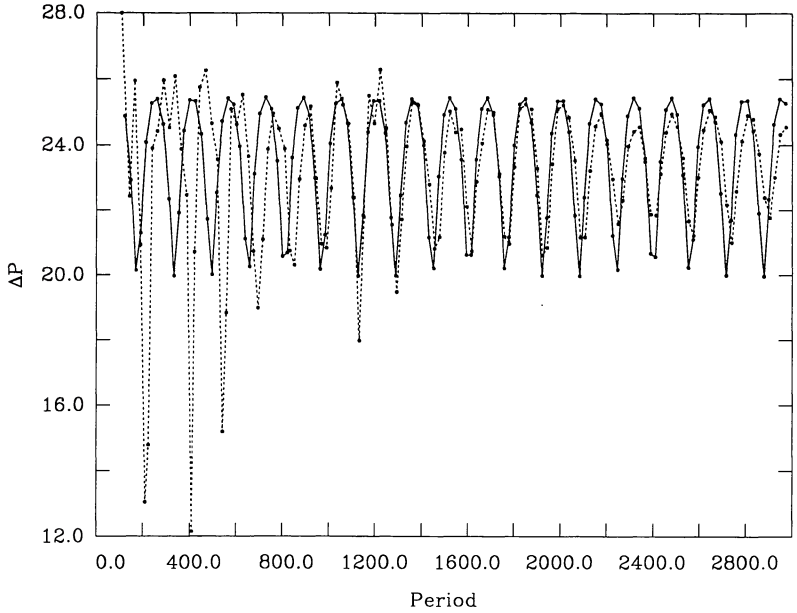

FIG. 12.—Comparison of the period distribution (in a period spacing vs. period diagram) of $l = 3$ modes for our reference model (*dotted curve*) with that predicted by our asymptotic approach (*solid curve*).

transition zone. By contrast, our asymptotic model idealizes the transition zone as a perfect discontinuity, so the departure from period uniformity is, on the average, the same (i.e., wavelength-independent) for all trapped (and confined) modes in that case.

Second, the period spacing between trapped modes (the interval between minima) is not uniform for low-k modes in the exact calculations. As expected (and as clearly seen in the figure), this spacing tends toward a constant only in the asymptotic limit of high radial overtones (as assumed in our analytic model). For these high-k modes, however, the superficial hydrogen convection zone (completely ignored in our analytic model) starts to affect somewhat the period spacing. Moreover, there are also secondary features in the dotted curve which are caused by residual trapping effects in the reference model. For example, the amplitude of the excursions in ΔP varies even for long-period modes, and there is even a hint of a beating phenomenon in the dotted curve. Of course, these residual effects cannot be explained within the framework of our simplified asymptotic approach. Nevertheless, we find that the *essential* features of the nonuniform period distribution of our stratified stellar model are very well accounted for by our asymptotic theory. Given that the confrontation of the results in a ΔP versus P diagram highly magnifies the "defects," we conclude, in fact, that the agreement shown in Figure 12 is *most* gratifying.

In the remainder of this section, we verify that the parameters Π_0, Π_H, n_e, and α^2—which we have empirically found to best fit the exact period distributions of stellar models—are physically meaningful. We thus estimate these parameters solely (when possible) on the basis of the structural properties of our evolutionary models and compare those values with the empirically determined ones.

The first parameter, Π_0, is readily available from a stellar model through a simple integration from the center to the surface (cf. eq. [39]). For the reference model, this integration gives $\Pi_0 = 81.13$ s, $\sim 1.8\%$ away from the value $\Pi_0 = 79.69$ s obtained by averaging period spacings between trapped modes with $i \geq 4$ in the period interval 0–1400 s (see above). We note that the difference would decrease to only 0.2% if we were to compare the integrated value of Π_0 with $\Pi_0 = 80.95$ s obtained by considering only trapped modes with $k \geq 70$ in the reference model. This improved agreement reflects the fact that the latter estimate is more representative of the fully asymptotic regime, on which our analytic approach is based. We have reported in column (2) of Table 7 the values of Π_0 obtained through direct integration from our evolutionary models. A comparison with Table 6 indicates that the differences in Π_0 are typically of the order of a few percent. We can observe that the empirical values of Π_0 (Table 6) are systematically smaller than the exact values (Table 7), reflecting, once again, the presence of small departures from the asymptotic regime in the

TABLE 7

PARAMETER VALUES OBTAINED DIRECTLY FROM EVOLUTIONARY MODELS

$T_{\rm eff}$ (K) (1)	Π_0 (2)	Π_H (3)	n_e (4)	α^2 (5)
15587	71.88	483.3	2.79	2.26
14807	74.01	489.7	2.70	2.54
13969	76.54	500.2	2.60	2.34
13239	78.75	505.6	2.50	2.40
12518	81.13	511.3	2.40	2.37
11833	83.85	522.0	2.16	2.43
11377	85.95	537.9	2.09	2.43
11134	87.36	557.0	2.04	2.43
10925	88.92	587.8	2.03	2.48
10568	91.26	623.3	2.00	2.51
9999	94.44	655.7	1.97	2.48

period distributions even for modes with $i \geq 4$. The behavior of Π_0 with respect to changes in model quantities (in particular, the monotonic increase of Π_0 with decreasing $T_{\rm eff}$ observed in Tables 6 and 7) has been discussed at length by Tassoul et al. (1990) and will not be repeated here. We refer the interested reader to that paper for more details.

The direct computation of the second parameter, Π_H, from a stellar model is made somewhat uncertain by the fact that we have to idealize a composition transition zone of finite width as a perfect discontinuity in order to make the comparison with the results of our asymptotic theory. In effect, we have to find the location of an "effective" composition interface in the model. The problem is vividly illustrated by the dashed line in Figure 1, which shows the running integral

$$\Pi_H = 2\pi^2 \left[\int_d^1 (|N|/x)\, dx \right]^{-1}$$

(eq. [40]) as a function of $\log q$ in our reference model. For $\log q = 0$, $d = 0$ and the running integral reduces to $\Pi_H = \Pi_0 = 81.13$ s, as expected. If, for the present needs, we define the base of the H/He composition transition zone at the point where the mass fraction of helium Y is equal to 0.999, and the top of the transition zone at the point where $Y = 0.001$ (see, e.g., Fig. 30*a* of Tassoul et al. 1990 for the profile of Y in a stratified white dwarf model), we find that Π_H varies from 372.5 to 742.5 s in going from the base to the top of the zone. Clearly, we must find an appropriate definition of the effective interface to derive more accurate values of Π_H from the models.

From the structural properties of a model alone, it is impossible to find the location of the effective interface; that information is contained in the period distribution. In that sense, and contrary to the case of the parameter Π_0 above, we cannot find independent estimates of Π_H based, on the one hand, on the structural properties and, on the other hand, on the pulsation properties of a model. We have therefore searched for an appropriate criterion using both sets of properties. Specifically, we have compared the Π_H values obtained from the period spectra of trapped modes for a very large set of models with different masses, composition layerings, convective efficiencies, and effective temperatures (taken from the adiabatic survey of Brassard et al. 1991d) with the values computed directly from equation (40), but with various ad hoc choices of the location (d) of the effective interface. Taking also the behavior of the eigenfunctions into account (see discussion in § 2 above), we find that a good choice for the effective interface is located at the point where the helium mass fraction Y is equal to 0.97. Although, once again, this criterion is not independent of the pulsation properties of a model (in particular, it is representative of trapped modes with $i \geq 4$ in the period window 0–2000 s), it has the merit of being universal with respect to model quantities such as mass, effective temperature, etc.

The condition $Y = 0.97$ corresponds to a point immediately below the H/He composition spike in the Brunt-Väisälä frequency distribution of a stratified white dwarf model. This is illustrated by the vertical dotted line in Figure 1, which applies to the reference model. The effective interface in this model is thus located near $\log q \simeq -9.5$. The value of Π_H corresponding to this effective interface is 511.3 s (horizontal dotted line in the figure). Column (3) of Table 7 contains the values of Π_H obtained similarly by combining equation (40) with the criterion Y(interface) = 0.97 for the evolutionary models which we have considered. A comparison with Table 6 indicates typical differences of a few percent only.

To complement the detailed discussion of Tassoul et al. (1990) on the behavior of Π_0 with respect to changes in various model parameters, we open a parenthesis here to review briefly the behavior of Π_H. As above, all the values of Π_H used in the present discussion come directly from integrating in the various models (eq. [40]), with the criterion Y(interface) = 0.97. Figure 13 shows the behavior of Π_H for models which differ in total mass ($M/M_\odot = 0.4$, 0.6, and 0.8) as a function of their hydrogen layer mass in the range $-13 \leq \log q(\mathrm{H}) \leq -4$. All those models have the same amount of helium [$\log q(\mathrm{He}) = -2$], are computed with ML1 convection, and have $T_{\rm eff} \simeq 12{,}000$ K. First, the general increase of Π_H with decreasing $\log q$(H) for a given mass reflects the fact that the integral $\int_d^1 (|N|/x)dx$ naturally diminishes as d is pushed toward the surface ($d \rightarrow 1$). The decrease of this integral is fairly rapid in the outermost layers ($\log q \lesssim -8$) despite the fact that $|N|$ keeps increasing toward the surface (see Fig. 1), because, at these shallow depths, the radial coordinate x has practically become constant. Hence, Π_H increases rapidly for $\log q \lesssim -8$. Second, for a given value of $\log q$(H), Π_H is larger for a less massive model. The first reason is that a less massive white dwarf (at a given $T_{\rm eff}$) has significantly lower values of the local gravity than a more massive star. Consequently, the Brunt-Väisälä frequency (see eq. [1]) in the less massive model is systematically lower, which implies a larger value of Π_H. As

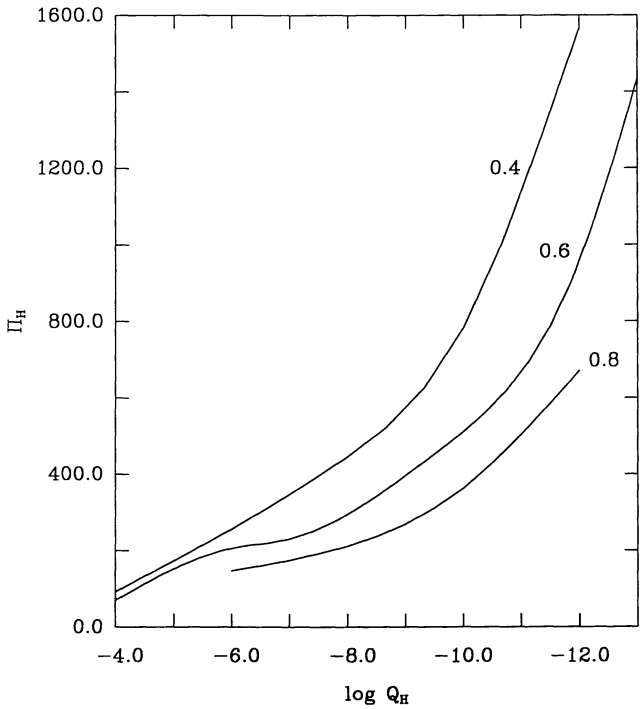

FIG. 13.—Behavior of the parameter Π_H as a function of the hydrogen layer mass $\log q$(H) for ~ 12,000 K, ML1 ZZ Ceti star models with $M/M_\odot = 0.4$, 0.6, and 0.8.

can be observed in Figure 13, the differences in Π_H become larger between models of different masses as log q(H) is decreased. Here the reason is that Π_H becomes increasingly sensitive to the details of the outermost layers, and, in particular, to the presence of a superficial hydrogen convection zone. It is well known that white dwarfs with low masses have much more extensive superficial convection zones than massive stars of comparable effective temperatures (Fontaine & Van Horn 1976). Hence, the integral $\int_d^1 (|N|/x)dx$ (which must be carried out over the radiative regions *only*) is further reduced in a less massive object, and this leads to a larger value of Π_H for such a star.

The continuous curves in Figure 14 show the behavior of Π_H in evolving 0.6 $M_\odot$ stratified white dwarf models [log q(He) = −2, ML1 convection] with different hydrogen layer masses. The evolution follows vertical trajectories in this diagram. Three values of the effective temperature are considered: $T_{\rm eff} \simeq$ 14,000, 12,000, and 10,000 K. The curves illustrate the monotonic increase of Π_H with decreasing $T_{\rm eff}$ in an evolving model, a trend already obvious in column (3) of Table 7, for example. This monotonic behavior is easily explained: as cooling proceeds, the star becomes more degenerate, the Brunt-Väisälä frequency decreases overall, and this translates into an increasing value of Π_H. We also note that, for a given evolving model, the increase in Π_H is more rapid for the lower temperature. In this case it is the development of the superficial hydrogen convection zone resulting from cooling which is responsible for this behavior: the integral $\int_d^1 (|N|/x)dx$ must again be carried out over radiative regions only, and the development of a convective zone will therefore result in a lower value of the integral and a higher value of Π_H. For the same reason given above

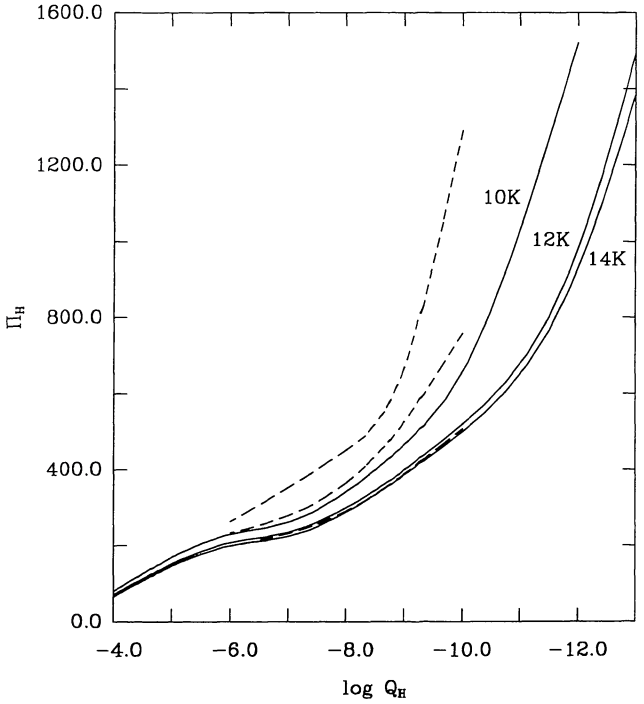

FIG. 14.—Same as Fig. 13, but for 0.6 $M_\odot$, ML1 ZZ Ceti star models with $T_{\rm eff}(10^3\,{\rm K}) \simeq$ 10, 12, and 14 and ML1 (*solid curve*) and ML3 (*dashed curve*) convection.

(namely, the increased sensitivity of the integral to the details of the outer envelope), the differences in Π_H due to cooling are larger for the models with the less massive hydrogen layers. Finally, the dashed curves show the influence of ML3 convection for a smaller set of models. At $T_{\rm eff} \simeq$ 14,000 K, there is practically no difference in the extent of the hydrogen convection zone and the integral $\int_d^1 (|N|/x)dx$ is essentially the same for the two sets of models. As a consequence, Π_H is very nearly the same, as can be seen by the near-coincidence of the dashed and continuous curves for that temperature. With cooling, ML3 convection leads to the formation of a more extended convection zone, the integral is obtained over a smaller (radiative) region, and Π_H is increased. Remembering that Π_H is a measure of the period spacing between trapped modes, we can summarize the present discussion in the following way. All other things being equal, the period spacing between trapped modes increases with (1) decreasing mass, (2) decreasing hydrogen layer mass, (3) decreasing effective temperature, and (4) increasing convective efficiency. This explains *all* the trends which characterize our semianalytic formula above (eq. [28]).

We now turn to the evaluation of the third parameter, n_e, directly from the properties of a stellar model. In the present context, n_e represents the "effective polytropic index" of the outer hydrogen layer (Tassoul 1980). Contrary to the deep degenerate interior of a white dwarf where the polytropic approximation can justifiably be made, however, the *outer layers* of a white dwarf star are not particularly well represented by a polytropic structure of constant index. Hence, n_e must be understood as some kind of average polytropic index which characterizes the outer layer as a whole. To obtain an estimate of n_e directly from a model, we combine the equation of hydrostatic equilibrium with the polytropic equation of state (eq. [4]). Assuming that n_e = constant and neglecting the variation of gravity in the hydrogen layer (an excellent approximation here), we find the following linear relation between the logarithm of the density, the logarithm of the depth from the surface, and the polytropic index,

$$\log \rho \propto n_e \log (R - r)\,. \tag{56}$$

Guided by this result, we have fitted in a least-squares sense (linear regression) the values of log ρ versus log $(R - r)$ between the H/He interface (Y = 0.97) and the surface of a model. Although, as expected, the correlation coefficient is not particularly impressive (because the envelope structure is not well represented by eq. [56] in its details), the procedure gives a reasonable estimate of an *average* value of n_e. Results are given in column (4) of Table 7 for the evolutionary models of interest. Note that the systematic decrease of n_e with decreasing $T_{\rm eff}$ in these models is due to the presence of a growing superficial hydrogen convection zone in which the "local" polytropic index plummets to very low values, thus biasing the average n_e toward smaller values. This sensitivity to convection may turn out to be a useful property in the interpretation of observed period spectra as discussed below.

It is possible to find other ways for estimating an average value of n_e than the procedure we followed here; the results should be fairly similar (to within 50%), however. In any case, we find that the actual results are already quite satisfactory

considering the basic simplicity of our asymptotic theory. Indeed, without considering further complications or restrictions, we find that the average value of the effective polytropic index in Table 7 is $n_e = 2.30 \pm 0.31$, consistent within 1 standard deviation with the average value $n_e = 2.69 \pm 0.12$ obtained from Table 6. Noting further that the entries for n_e in the two tables tend to be quite similar for the hotter models (where hydrogen convection is practically negligible), we find effectively that the agreement between the two sets of values is quite satisfactory.

Finally, we consider the fourth parameter, α^2, which measures the strength of the discontinuity in the Brunt-Väisälä frequency due to the H/He transition zone. Here we could expect difficulties of the same nature as those which we encountered when dealing with Π_H because our asymptotic theory has idealized a transition zone of finite width as a perfect discontinuity. Fortunately, however, the considerations put forward in the previous section clearly indicate that the relevant location for estimating α^2 is on the helium side of the H/He composition spike in the Brunt-Väisälä frequency distribution. Hence, in practice in a model, we simply estimate α^2 from the contrast between the maximum value of the spike and the first secondary maximum on the helium side of the transition zone. For example, in Figure 1 the maximum value of $\log N^2$ at the top of the H/He spike is 2.72, while the value of $\log N^2$ at the secondary maximum located near $\log q \simeq -9.8$ is 1.97. This leads to an estimate $\alpha^2 = (10^{2.72}/10^{1.97})^{1/2} = 2.37$ for the reference model. Values of α^2 obtained in a similar way are given in column (5) of Table 7 for the other models. As expected, because of the slow evolution of the equilibrium diffusion profile in this temperature range, there is no real trend with effective temperature, and we find an average value $\alpha^2 = 2.43 \pm 0.08$. This is consistent (within 1 standard deviation) with the average value of Table 6, $\alpha^2 = 2.28 \pm 0.08$, which is based on the full period spectra.

We have therefore established in this section that (1) the exact period distributions (the full one and that of trapped modes) of detailed evolutionary models can satisfactorily—and even accurately in the case of trapped modes—be reproduced in terms of four parameters only: Π_0, Π_H, n_e, and α^2, and (2) the derived values of these parameters obtained from empirical fits to exact period spectra are physically meaningful in the sense that they do correspond to model properties. This raises the interesting prospect of being able to use a very simple theory (the asymptotic approach developed in the previous section) as a guide for interpreting observed period distributions in ZZ Ceti stars and for inferring some of their fundamental properties. In this respect, the four parameters of the theory can be quite useful. For instance, we have shown (see also Tassoul et al. 1990) that both Π_0 and Π_H depend on the total mass of the star, the hydrogen layer mass, the effective temperature, and, to a lesser extent, the convective efficiency. The dependences on model quantities are different, with Π_0 being particularly sensitive to the total mass, while Π_H is particularly sensitive to the hydrogen layer mass. Likewise, the parameter n_e can be used as a measure of the depth of the hydrogen convection zone in a ZZ Ceti star. For example, Table 7 indicates that $n_e \simeq 2.40$ in our reference model computed under the assumption of ML1 convection. As a comparison, a similar model differing only from the reference model by the assumption of ML3 convection (thus giving rise to a deeper hydrogen convection zone) has a value of the effective polytropic index $n_e \simeq 0.55$. This sensitivity may provide a useful indication of the depth of the convection zone. Note, however, that the "effective range" of n_e is 2 (see eq. [37]). Finally, the parameter α^2 is also of great interest because it is directly related to the diffusion processes which specify the actual composition profile in the H/He transition zone. Typical values of α^2 are around 2.4 if the composition profile is obtained from diffusive equilibrium induced by ordinary diffusion in white dwarf stars. In a numerical experiment in which the scale height of the composition transition zone was artificially reduced by a factor of 10 (the T60510C1 models of Tassoul et al. 1990), Brassard et al. (1991d) find that α^2 increases to ~ 7.5, thus providing a useful diagnostic for measuring the thickness of the H/He transition zone.

In the next section we illustrate how our asymptotic theory can be used for interpreting the period spectra of ZZ Ceti stars. Before we do this, however, we remind the reader that our asymptotic model is highly idealized, and, in particular, is based on the assumption that there is only *one* composition discontinuity in the star. Consequently, our model (in its present form) cannot be used, for example, to study the simultaneous effects of trapping due to *both* the H/He and the He/C transition zones in ZZ Ceti stars. It should be straightforward (but probably tedious) to generalize the algebra presented in § 4 to the case of two discontinuities. However, we feel that this is hardly worth the effort because detailed numerical calculations (cf. Brassard et al. 1991d) show that the nonuniformities of the period distribution caused by trapping at the He/C interface in a ZZ Ceti star model are much smaller than those caused by trapping at the H/He interface. As briefly alluded to above, this is because the He/C interface is (or at least is believed to be) located much deeper in the star, in a region which does not carry much weight in terms of period formation. While this circumstance simplifies considerably the interpretation of observations, it also means that an estimation of the helium layer mass q(He) in a ZZ Ceti star will probably be very difficult to obtain.

6. A PROCEDURE FOR INTERPRETING THE OBSERVED PERIOD SPECTRUM OF A ZZ CETI STAR IN TERMS OF MODE TRAPPING

The paucity of well-resolved excited modes with amplitudes larger than typical detection levels in the majority of ZZ Ceti stars makes it currently impossible to interpret their observed period spectra through direct comparison with model calculations. This is because the full theoretical g-mode spectra are so densely packed, while, in comparison, the observed spectra are so poorly populated, that *many* identifications are possible: several stellar models, sometimes with vastly different parameters, can account equally well for the sparse period data. If, in contrast to purely geometrical or detection-threshold effects, this relative poverty of the observed period distributions is due to an efficient filtering mechanism (as strongly suggested by the previous work of many workers on mode trapping induced by compositional layering), then the situation brightens up considerably because only certain selected modes are expected to remain in the theoretical g-mode spectra. In that case, the

probability of obtaining multiple, nonunique solutions or identifications diminishes considerably. An attractive working hypothesis is therefore the assumption that *all* (or at least most) of the observed modes in a ZZ Ceti star are actually modes trapped in the outer hydrogen layer. Obviously, this assumption cannot be verified a priori in a given ZZ Ceti star, but its internal consistency can be verified after the fact.

In the following, we will use the analytic tools developed in this paper to establish a procedure for analyzing the observed period distributions of ZZ Ceti stars in terms of mode trapping. Unfortunately, we cannot yet apply this procedure to a specific star because a critical look at the available published data on ZZ Ceti variables reveals that such an interpretation would currently be premature. The simplest ZZ Ceti stars are the low-amplitude (probably linear) pulsators which show but a handful of modes with amplitudes larger than typical detection limits in the Fourier spectra of their light curves. Typically, the number of detected modes (2–4) in those stars remains too small for our interpretation procedure to be useful, because, as we will show below, the procedure relies heavily on period spacings and period ratios. Our newly initiated search for low-amplitude modes in pulsating white dwarfs at the Canada-France-Hawaii Telescope promises to be quite helpful here (for a recent example see Fontaine et al. 1991b), and we are planning among other things to investigate systematically the known sample of ZZ Ceti stars.

The large-amplitude pulsating DA white dwarfs usually do show enough peaks in the Fourier spectra of their light curves for the procedure to work in principle. However, in that case, the question of untangling real modes from aliases becomes important. The situation has been well summarized by Nather et al. (1990), who have proposed the Whole Earth Telescope concept as a solution to this problem, but data for most ZZ Ceti stars remain to be obtained. An additional difficulty with the large-amplitude variables is that nonlinear effects lead to the appearance of harmonics and cross-frequencies (linear combination of basic frequencies) in the Fourier domain (cf. Brickhill 1991). It becomes difficult in such cases to discriminate between the frequency peaks corresponding to real, basic pulsation modes, and those which result from the nonlinear superposition of modes and which, themselves, do *not* correspond to additional individual pulsation modes. The difficulty is exacerbated by the fact that the period spectrum of trapped modes only is *still* sufficiently dense that chance occurrences between real frequency peaks can mimic surprisingly well the nonlinear effects (even the harmonics) just discussed. We show an example of this in Appendix B, where the trapped-mode period spectrum of our reference model is considered. The solution to this dilemma will again be obtained from very high temporal resolution observations such as those reached in Whole Earth Telescope campaigns.

In the (temporary) absence of sufficiently detailed data for ZZ Ceti stars, we will idealize the (complex) observational situation by using our reference model as an example of an "observed" period spectrum. Of course, in doing so, we assume that we have successfully avoided all the pitfalls—and they are numerous—associated with the identification of periods corresponding to individual pulsation modes present in the light curve. We thus will now pretend that our observational input consists of 17 periods (col. [4] of Table 4). Apart from the basic assumption that these are all trapped modes and the reasonable expectation (although this is not restrictive) that they have $l \leq 3$, we assume that nothing else is known about these modes.

The first step is to build period ratios from the observed period spectrum (see Table 8) in order to take advantage of our asymptotic results, which suggest that (1) the periods of trapped modes with the same value of i (they also must have approximately the same value of k) are related by (cf. eq. [48] or eq. [28])

$$\frac{P_{il}}{P_{il'}} \simeq \left[\frac{l'(l'+1)}{l(l+1)}\right]^{1/2}, \tag{57}$$

and (2) the periods of trapped modes with the same value of l are related by (cf. eq. [28])

$$\frac{P_{i'l}}{P_{il}} \simeq \frac{\lambda_{i'}}{\lambda_i}. \tag{58}$$

From equation (57), the ratios of interest for modes with $l = 1$, 2, and 3 are $P_{i2}/P_{i3} \approx 1.41$, $P_{i1}/P_{i2} \approx 1.73$, and $P_{i1}/P_{i3} \approx 2.45$. Combining the results of Table 1 for the first six trapping coefficients with equation (58), we also report in Table 9 the expected period ratios $P_{i'l}/P_{il}$. Note that two of these ratios (1.39 and 1.74) are quite close to those associated with modes with different l-values, so some care must be taken here in order to avoid confusion. In practice, cross-referencing usually permits the correct identification.

From Table 8 it is relatively easy to first group the periods in sequences with different values of l. For example, the ratio 1.39 ($\simeq$1.41) in the second column suggests that the 223.52 s period is an $l = 3$ mode, while the 311.32 s period is an $l = 2$ mode. In the same column, the ratio 2.46 ($\simeq$2.45) is consistent with the possibility that the 223.52 s period is indeed an $l = 3$ mode, while the 550.32 s period is possibly an $l = 1$ mode. These three modes must therefore have the same value of i but different values of l. Making no reference whatsoever to the known quantum numbers of the "observed" periods (cf. Table 4), we have worked our way through Table 8 finding 12 period ratios very close (within $+0.04/-0.02$) to the expected ratios for modes with the same values of i but with $l = 1$, 2, or 3. On this basis, we are able to classify 15 modes in three sequences with different l-values. We are left with two periods (1132.49 s and 1294.75 s) which we immediately assign to the $l = 3$ sequence on the basis of the average period spacing ($\sim$155 s) obtained from the six periods already assigned to that sequence. The classification of the observed periods in terms of l is presented in Table 10. The periods found on the same line correspond to modes with the same value of i. We note that our assignment of modes in terms of l (as compared with the exact results of Table 4) is almost perfect; only the nearly equal periods 990.88 s and 998.31 s have been inverted. This situation due to an accidental degeneracy of periods is unavoidable here. In Table 8 the ratio of the 990.88 s period to the 696.05 s period is 1.42, closer to the expected value of 1.41 than the ratio 998.88/696.05 = 1.43, which explains why we chose the 990.88 s period instead of the 998.88 s period as the $l = 2$ mode. On the other hand, we can also point out that the ratio 1388.05/990.88 = 1.40 is closer to 1.41 than the ratio

TABLE 8

PERIOD RATIOS FROM "OBSERVED" PERIOD SPECTRUM

	PERIOD															
PERIOD	223.52	311.32	421.62	550.32	557.67	587.96	696.05	779.46	853.98	990.88	998.31	1034.98	1132.49	1222.25	1294.75	1367.73
311.32	1.39															
421.62	1.89	1.35														
550.32	2.46	1.77	1.31													
557.67	2.49	1.79	1.32	1.01												
587.96	2.63	1.89	1.39	1.07	1.05											
696.05	3.12	2.24	1.65	1.27	1.25	1.19										
779.46	3.49	2.50	1.85	1.42	1.40	1.33	1.12									
853.98	3.82	2.74	2.03	1.55	1.53	1.45	1.23	1.10								
990.88	4.43	3.18	2.35	1.80	1.78	1.69	1.42	1.27	1.16							
998.31	4.47	3.21	2.37	1.81	1.79	1.70	1.43	1.28	1.17	1.01						
1034.98	4.63	3.32	2.45	1.88	1.86	1.76	1.49	1.33	1.21	1.04	1.04					
1132.49	5.07	3.64	2.69	2.06	2.03	1.93	1.63	1.45	1.33	1.14	1.13	1.09				
1222.25	5.47	3.93	2.90	2.22	2.19	2.08	1.76	1.57	1.43	1.23	1.22	1.18	1.08			
1294.75	5.79	4.16	3.07	2.35	2.32	2.20	1.86	1.66	1.52	1.31	1.30	1.25	1.14	1.06		
1367.73	6.12	4.39	3.24	2.49	2.45	2.33	1.96	1.75	1.60	1.38	1.37	1.32	1.21	1.12	1.06	
1388.05	6.21	4.46	3.29	2.52	2.49	2.36	1.99	1.78	1.63	1.40	1.39	1.34	1.23	1.14	1.07	1.01

1388.05/998.31 = 1.39, which implies that the 990.88 s period should, on this basis, now be assigned the value $l = 3$. Of these two equally valid choices, we had originally picked the first one, so we will stick to that (largely inconsequential) choice in what follows.

The actual assignment of the i-values is most easily made by first using a trial value (e.g., $i = 1$) for the modes on the first line in Table 10, and then checking, in a given column, whether the period differences between consecutive modes are compatible with a series with $\Delta i = 1$. It is quite possible that, in a real experimental situation, consecutive trapped modes may not all be detected. This would immediately show up in terms of unequal period spacing in a given column. The assignment based on period spacings can also be checked by comparing period ratios of modes found in the same column of Table 10 with the ratios given in Table 9. For example, we find that the ratios of the periods listed on the second line of Table 10 to those listed on the first line are 1.88 ($l = 1$), 1.89 ($l = 2$), and 1.89 ($l = 3$), all close to the expected ratio 1.97 (see Table 9) between modes with the same l-value but with $i = 2$ and $i = 1$. Likewise, the ratios of periods found on the third and second lines in Table 10 are 1.32 ($l = 1$), 1.33 ($l = 2$), and 1.32 ($l = 3$), close to the expected value 1.39 between modes with $i = 3$ and $i = 2$. The ratios of periods found on the fourth and third lines in Table 10 are 1.27 ($l = 2$) and 1.25 ($l = 3$), close to the expected value 1.26 between modes with $i = 4$ and $i = 3$. By pursuing this process, it is relatively easy to obtain the final i assignment given in the first column of Table 10. We note that the period ratios for the higher i modes become less useful for discriminating between modes. Also, we do not have trapping coefficients for $i = 7$ and $i = 8$, but, as pointed out previously, the average period spacing derived from the first six modes with $l = 3$ ($\sim$155 s) clearly shows that the assignment of the last two modes with $l = 3$ in Table 10 is correct. It is important to note here that the dispersion of period ratios based on different values of i (for the same l) is much larger than that based on different values of l (for the same i). Hence, it is essential that the l assignment be carried out *before* the i assignment is attempted.

TABLE 9

RATIOS OF THE FIRST SIX TRAPPING COEFFICIENTS

i	λ_i	$i = 1$, $\lambda_i = 2.28$	$i = 2$, $\lambda_i = 4.49$	$i = 3$, $\lambda_i = 6.23$	$i = 4$, $\lambda_i = 7.83$	$i = 5$, $\lambda_i = 9.18$
2	4.49	1.97				
3	6.23	2.73	1.39			
4	7.83	3.43	1.74	1.26		
5	9.18	4.03	2.04	1.47	1.17	
6	10.44	4.58	2.33	1.68	1.33	1.14

At this stage, we can now estimate Π_H by averaging the period spacings between the consecutive trapped modes:

$$\Pi_H \simeq \frac{1}{N} \sum_{l=1}^{3} \sum_{i} (P_{i+1l} - P_{il})[l(l+1)]^{1/2}, \qquad (59)$$

where N is the total number of period spacings available. From the data of Table 10, we find $\Pi_H = 536.0$ s. We note here that the period spacing between the first and second trapped modes is particularly large (compared with the mean), which biases Π_H toward relatively large values. In fact, the inclusion of the first trapped mode is already quite questionable because our approach is expected to be valid only in the asymptotic limit of high radial overtones, in which case the period spacing between consecutive trapped modes is predicted to be constant. Of course, the period spacings between the other trapped modes are not exactly uniform, but the case involving the first trapped modes is particularly outstanding. Hence, by excluding the $i = 1$ modes in the averaging process of equation (56), we now find $\Pi_H = 495.9$ s, in much better agreement with the value $\Pi_H = 504.8$ s obtained previously for the "target" star (cf. Table 5) based on the exact mode assignment for the period spectrum and using only modes with $i \geq 4$. In practice, the

TABLE 10

MODE IDENTIFICATION FOR "OBSERVED" PERIOD SPECTRUM

	$l = 1$			$l = 2$			$l = 3$		
i	Period (s)	Δk	k	Period (s)	Δk	k	Period (s)	Δk	k
1	550.32		8	311.32		7	223.52		7
		8			8			8	
2	1034.98		16	587.96		15	421.62		15
		6			6			6	
3	1367.73		22	779.46		21	557.67		21
					6			6	
4				990.88		27	696.05		27
					7			7	
5				1222.25		34	853.98		34
					5			6	
6				1388.05		39	998.31		40
								6	
7							1132.49		46
								7	
8							1294.75		53

$i = 1$ modes should therefore not be included in the evaluation of Π_H. Although the asymptotic approximation would be even better verified if we would restrict the averaging process to modes with $i \geq 4$, as we have done in the theoretical discussion above, we probably cannot afford in practice to drop the modes with $i = 2$ and $i = 3$ because the observed period spectrum may not be rich enough. To mimic as closely as possible a real experimental situation, we only drop the $i = 1$ modes.

Beyond the l and i identifications, the determination of the parameter Π_H is the only useful result which can be obtained (although a crude estimate of n_e is also possible; see below) if the only information that we have about a target star is a distribution of periods for trapped modes. Because, as we have seen previously, Π_H depends on several stellar parameters, we need additional independent information about the star to exploit fully the potential of asteroseismology. This requirement is the primary reason which motivates the ongoing effort at Montreal to combine detailed model atmosphere calculations with time-averaged spectroscopic and photometric observations of ZZ Ceti stars for deriving the atmospheric properties of these objects (Wesemael, Lamontagne, & Fontaine 1986; Lamontagne, Wesemael, & Fontaine 1987; Daou et al. 1990; Wesemael et al. 1991; Bergeron, Wesemael, & Fontaine 1992). From studies of that sort, we can derive effective temperatures, gravities, and possibly convective efficiencies (see Bergeron et al. 1992). Coupled with appropriate mass-radius relationships coming from detailed evolutionary calculations, reasonable estimates of the masses of ZZ Ceti pulsators can also be obtained. Hence, to proceed further in the present discussion, we now assume that we have obtained independent estimates of the mass ($\sim 0.6\ M_\odot$), the effective temperature ($\sim 12{,}500$ K), and the convective efficiency ($\sim$ML1) of the target star.

The discussion could now end by combining these stellar parameters, the l and i mode identifications, and our semianalytic formula (eq. [28]) to derive $q(\mathrm{H})$, the most interesting stellar property that can be obtained from ZZ Ceti star seismology. Using the 15 modes in Table 10 for which we have values of the trapping coefficients ($i \leq 6$), we obtain an average value of the hydrogen layer mass $\log q(\mathrm{H}) = -10.03 \pm 0.15$, quite close to the exact value of -10.0. Figure 15 illustrates the trapped-mode period spectrum ($l = 1$, 2, and 3), predicted by our semianalytic formula for ZZ Ceti stars with $M = 0.6\ M_\odot$, $T_{\rm eff} = 12{,}500$ K, and ML1 convection as a function of the hydrogen layer mass. The dots correspond to the 17 periods of our "target" star; they are located at the level $\log q(\mathrm{H}) = -10.03$ corresponding to the average value which we have found. The deviations of the dots from the curves are representative of the accuracy of our semianalytic approach. Note that two periods do not match at all; these correspond to modes

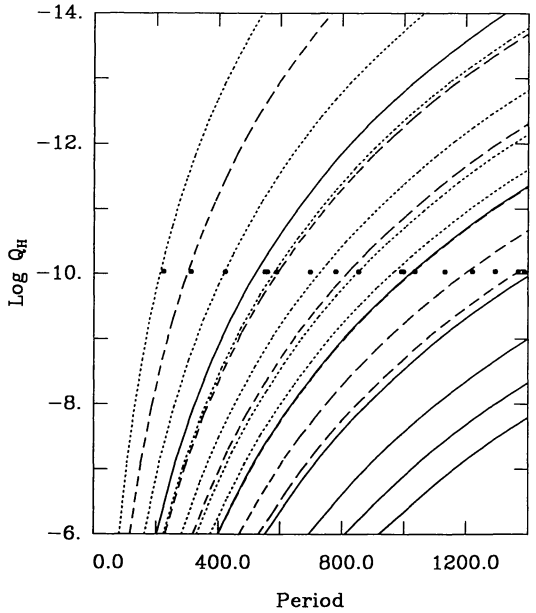

FIG. 15.—Period spectrum for trapped modes in terms of the hydrogen layer mass as predicted by our semianalytic formula for 12,500 K, ML1, 0.6 $M_\odot$ DA white dwarf models. The dotted, dashed, and solid lines refer, respectively, to modes with $l = 3$, $l = 2$, and $l = 1$. The dots give the trapped-mode periods of our "observational" data.

with $i = 7$ and $i = 8$, not covered by our semianalytic formula. Note also that "Elvis hair style" diagrams such as the one shown in Figure 15 are quite useful for rapid diagnostics of the observed period spectra of ZZ Ceti stars in terms of trapped modes. With the help of such diagrams, it is very easy to verify whether or not a given period distribution bears the signature of mode trapping and, if it does, to infer an approximate value of the hydrogen layer mass in the star. Some of the results of Kawaler (1991) and Kawaler & Weiss (1991) using similar diagrams already suggest (despite current observational limitations) that many ZZ Ceti stars indeed show the signature of mode trapping.

As an alternative to using our semianalytic formula, we can estimate $q(\mathrm{H})$ by interpolation in the grid of ZZ Ceti star models of Tassoul et al. (1990), given that $\Pi_{\mathrm{H}} = 495.9$ s and that the mass, the effective temperature, and the convective efficiency of the star are known. More expeditiously here, we find by reading directly in Figure 14 (valid for 0.6 $M_{\odot}$ models) that a ZZ Ceti star with $\Pi_{\mathrm{H}} \simeq 500$ s, $T_{\mathrm{eff}} \simeq 12{,}500$ K, and ML1 convection has a hydrogen layer mass $\log q(\mathrm{H}) \simeq -9.8$. This is satisfactorily close to the exact value $\log q(\mathrm{H}) = -10.0$.

We can further proceed by using a similar method for estimating Π_0. From Figure 37 of Tassoul et al. (1990), we find that a 12,500 K, 0.6 $M_{\odot}$, ML1 ZZ Ceti star model with $\log q(\mathrm{H}) \simeq -9.8$ has a value $\Pi_0 \simeq 82$ s. Note that Π_0 cannot be inferred directly from the 17 periods available. If, for example, we use a Kolmogorov-Smirnov test to search for potential constant period spacings in our observed period distribution (see Kawaler 1988), we find, as expected, the strongest signal at a spacing corresponding to $\Pi_{\mathrm{H}} \simeq 500$ s, but there is no significant signal in the region where Π_0 could potentially be found. The physical reason here is that the trapped-mode period spectrum does not contain useful information about the parameter Π_0; the periods of trapped modes are *not* uniformly distributed on the scale of Π_0.

With the values of both Π_{H} and Π_0 known, we can now consider the final step in mode identification, i.e., finding the k-values of the individual modes. To do this, we again must make the crude assumption that, in a first approximation, the periods of trapped modes are given by *both* equation (41) (no trapping) and equation (42) (perfect trapping). From the ratio of Π_{H} and Π_0, we find that the average value of the wavenumber spacing between trapped modes is $\overline{\Delta k} \simeq 496/82 \simeq 6$. We can improve on that by computing (to the nearest integer) the spacing between consecutive trapped modes with the same value of l. From equation (41), we find

$$\Delta k = (P_{i+1l} - P_{il}) \frac{[l(l+1)]^{1/2}}{\Pi_0} . \tag{60}$$

Using $\Pi_0 \simeq 82$ s, we obtain the Δk values given in Table 10. We now need a zero-point value for k, which we obtain by again using equation (41). To do this, however, we need an estimate for n_e. We obtain this estimate by using equation (42), which gives

$$n_e = \frac{2P_{il}[l(l+1)]^{1/2}}{\Pi_{\mathrm{H}}} - 2i + \frac{1}{2} . \tag{61}$$

Using $\Pi_{\mathrm{H}} \simeq 495.9$ s, an average over 14 modes given in Table 10 gives $n_e \simeq 2.35$. In the averaging process, we have specifically excluded the $i = 1$ modes because their associated n_e values are substantially ($\sim$30%) lower than the mean value; by contrast, the value of n_e are the same within 8% for the other modes. From equation (41), we finally obtain

$$k = \frac{P_{il}[l(l+1)]^{1/2}}{\Pi_0} - \frac{l + n_e + \frac{1}{2}}{2} . \tag{62}$$

We have used equation (62) to estimate k (to the nearest integer) for the modes with $i = 2$ (we explicitly avoid the modes with $i = 1$), which we use as zero points. The results are reported in Table 10; coupled to the Δk values estimated previously, we obtain the other values of k given in the table. A comparison with the exact results given in Table 4 shows an excellent agreement. There is a systematic trend for the modes with $i = 1$, in the sense that our procedure leads to k-values which are larger by one unit as compared with the exact results. For the other modes, however, our k assignment is almost perfect. We note, in particular, that, had we chosen the 998.31 s period instead of the 990.88 s period as the $l = 2$ mode, the k assignment would have been perfectly correct for the $l = 2$ sequence.

From equation (48), we can finally obtain an estimate of α^2 through a two-dimensional χ^2 fit to the 17 periods (with α^2 and Π_{min} as free parameters), given that the modes have been identified (i, l, and k are known) and that we have a crude value of n_e ($\simeq$2.35). The χ^2 fit gives $\alpha^2 = 3.25$ and $\Pi_{\mathrm{min}} = 59.1$ s, the latter consistent with $\Pi_{\mathrm{min}} = 59.8$ s directly computed from Π_0, Π_{H}, and α^2. Not surprisingly, the derived α^2 is somewhat larger than the adopted value above (2.28) because our crude estimate of n_e is smaller than the "exact" value of 2.83. As we have discussed previously, there is a coupling (a negative correlation) between α^2 and n_e which we cannot undo on the basis of trapped modes only. The couple $[\alpha^2, n_e]$ that we have found is again located at the bottom of the χ^2 valley in Figure 11.

To conclude this section, we summarize the procedure which must be followed for interpreting the period spectra of ZZ Ceti stars under the assumption that the observed periods correspond to trapped modes only. From period ratios, the modes can be identified in terms of their l and i indices. From averaging period spacings, the parameter Π_{H} is derived. In this process, the modes with $i = 1$ should not be included, however. In our example, we found $\Pi_{\mathrm{H}} \simeq 495.6$ s, very close to the more appropriate asymptotic value ($i \geq 4$) $\Pi_{\mathrm{H}} \simeq 504.8$ s. In the absence of external constraints on the star to be analyzed, that is all the useful information that we can get out of the trapped-mode period spectrum. On the other hand, if we dispose of reasonable estimates of the total mass, the effective temperature, and (to a lesser extent) the convective efficiency of the star, we can directly infer the hydrogen layer mass $q(\mathrm{H})$, the most interesting quantity of ZZ Ceti star seismology. Either from our semianalytic formula or through the model integral Π_{H}, we have obtained a value of $\log q(\mathrm{H})$ very close to -10.0, the exact result. From the model integral Π_0, we can also estimate Π_0 given the known stellar parameters; we have found $\Pi_0 \simeq 82$ s, which is to be compared to the "exact" result, $\Pi_0 \simeq 79.69$ s. Mode identification can be finalized by (1) deriving the spacings Δk between modes belonging to the same l-se-

quence by using equation (41), and (2) finding zero points for k by again using equation (41), once n_e is known (in the process the modes with $i = 1$ should *not* be used as reference points; modes with $i = 2$ are suitable). We have found that the assigned values of k are essentially correct, except for the modes with $i = 1$ for which our estimated values of k are one unit too large. To arrive at the final step in the mode identification procedure, we have used a crude estimate of n_e based on equation (42). Again the modes with $i = 1$ should not be used here. We have found that the procedure *underestimates* the true n_e by $\sim 17\%$. Finally, using the derived mode identification and the estimate of n_e, equation (48) can be χ^2 fitted to obtain an approximate value for α^2. We have found that α^2 is *overestimated* by some 43% in this procedure. We suggest that corrections of that order be applied to obtain more physically meaningful values of n_e and α^2 in future analyses of real ZZ Ceti star data.

The ultimate test of the procedure is to find, among a bank of detailed numerical models, a model which has a period structure similar to that of the observed spectrum. This provides the final and necessary consistency check in the analysis. We have been working diligently to provide a suitable bank of models for such comparisons (the result of these efforts will be reported later). Quite early, however, it has appeared to us that the parameter space for DA white dwarf models is so vast that there is no hope of comparing the models directly with the observations. This is why the asymptotic theory developed here becomes so useful. We believe that the procedure we have just described is necessary to guide us in parameter space and lead us to a region where models have period spectra very similar to the observed spectra.

7. CONCLUSION

In this paper we have extensively studied the phenomenon of mode trapping caused by compositional layering in models of pulsating DA white dwarfs. This was motivated by the real possibility that most (if not all) pulsation modes detected in ZZ Ceti stars are actually modes which are trapped in the outer hydrogen layer. We began by describing the various effects of compositional layering on the pulsational properties of a representative ZZ Ceti star model. We have found that the presence of a H/He composition transition zone in the outer envelope of a DA white dwarf has a major influence on the period spectrum of the star. The change in composition in the H/He transition zone produces a spike in the Brunt-Väisälä frequency profile which pinches the eigenfunctions of all modes. Modes which happen to have nodes in the vicinity of the H/He interface ($y_1 \approx 0$, from above, and $y_2 \approx 0$, from below) tend to be reflected at this interface and are, consequently, mostly trapped in the outer hydrogen layer. The amplitudes of the eigenfunctions of such modes below the H/He interface are therefore much smaller than the amplitudes of more normal modes. It follows that trapped modes distinguish themselves by minimal kinetic energies and maximal first-order rotation coefficients. In addition, the region of period formation for trapped modes is usually located much higher (above the H/He interface) than that of other modes. This shift in the region of period formation from mode to mode produces a characteristic nonuniformity in the period distribution of a layered white dwarf model. In particular, trapped modes show minimal values in the ΔP versus P diagram. From an observational point of view, it is precisely the nonuniformity of the period spectrum which reveals the effects of compositional layering in ZZ Ceti stars. The location of the H/He interface in a model leaves a distinct signature on the period spectrum and bears directly on the question of the efficiency of mode trapping as a mode-selection mechanism. Models which are characterized by thick hydrogen layers show relatively small spacings between the periods of consecutive trapped modes. At the same time, these models are much less efficient at isolating trapped modes. Thus, a ZZ Ceti star which shows a period spectrum bearing the signature of mode trapping is unlikely to have a thick hydrogen layer.

We have developed analytic tools to understand the nonuniformity of the period spectra of pulsating DA white dwarf models. First, we have derived a semianalytic formula (eq. [28]) which can reproduce the periods of trapped modes to within several percent as compared with exact numerical calculations. The formula is based on the combination of a simple polytropic model with fits to detailed numerical calculations for a large number of models. It explicitly shows that the periods of trapped modes increase when (1) the total mass decreases, (2) the effective temperature decreases, (3) the hydrogen layer mass decreases, and (4) the convective efficiency increases. Our semianalytic formula is particularly useful for estimating quickly the hydrogen layer mass of a ZZ Ceti star given that the period of a trapped mode is known, that the mode has been identified in terms of its indices i and l, and that reasonable estimates are available for the stellar parameters.

Second, we have used the analytic expressions of Tassoul (1980) to investigate the full g-mode period spectrum of a stellar model containing a discontinuity (mimicking the H/He transition zone) in its Brunt-Väisälä frequency profile. The central result is contained in the transcendental equation (37) which gives the complete period spectrum of a model in the asymptotic limit of high radial overtones. The nonuniformity of the period distribution becomes apparent in this expression. By specializing to the case of trapped modes only, we have also derived a useful analytic expression for the periods of the modes (eq. [48]). In both cases, the results are expressed in terms of four parameters *only:* Π_0, Π_H, n_e, and α^2. Each of these parameters, in turn, depends on some structural properties of a stellar model. For instance, both Π_0 and Π_H are sensitive to the total mass (particularly Π_0), the effective temperature, the hydrogen layer mass (particularly Π_H), and the convective efficiency; n_e is sensitive to the depth of the outer hydrogen convection zone; and α^2 measures the thickness of the H/He transition zone.

We have carried out detailed comparisons of the predictions of our asymptotic model with the results of exact numerical calculations. We find that equation (48) can reproduce quite accurately the periods of trapped modes. The agreement is not so good if we compare the full period spectrum of a model with that predicted by equation (37), but this was fully expected considering the complexity of the model period spectrum and the approximations which have been made in deriving equation (37). Nevertheless, our simple analytic model accounts

very well for the *essential* features of the full period distribution, and the agreement must be considered as quite satisfactory.

Given the success of our analytic model at reproducing accurately the periods of trapped modes, we have proposed, on the basis of the model, a simple procedure for interpreting observational data in terms of mode trapping. Current available data on ZZ Ceti stars are of insufficient quality for this kind of analysis, but this is likely to change in the short-term future, thanks to newly initiated observational searches at high sensitivity and high temporal resolution. The prospect for inferring structural quantities from seismological data of white dwarfs is excellent.

Finally, we note that the asymptotic model which we have developed in this paper is not only useful, but also essential for understanding the results of detailed numerical calculations of the period spectra of ZZ Ceti stars. We will report in a forthcoming paper the results of such a survey.

We are grateful to M. Tassoul for useful discussions and comments on an early version of this manuscript. We also wish to thank A. Talon for providing continuous inspiration and insight to our work on white dwarf stars. This work was supported in part by the NSERC Canada and by the Fund FCAR (Québec). G. Fontaine also enjoyed the support of a Killam Fellowship.

APPENDIX A
RELATION BETWEEN THE SEMIANALYTIC AND THE ASYMPTOTIC MODEL

In appearance, the functional dependence of our semianalytic formula for the periods of trapped modes (eq. [17]) bears little resemblance to the results we have obtained from our asymptotic approach. We show here, however, that we can actually recover this dependence from our formula (42), which applies to perfectly trapped modes. From equation (42) we have

$$P_{il} = \left(2i + n - \frac{1}{2}\right) \frac{\pi^2}{[l(l+1)]^{1/2}} \int_d^1 \frac{|N|}{x}\, dx\,. \tag{A1}$$

For the simple polytropic model considered in § 3 and applicable to the outer hydrogen layer of a ZZ Ceti star, it is straightforward to show that the Brunt-Väisälä frequency is given by

$$|N| = \left(\frac{n - \tilde{n}}{1 - x} \frac{GM}{R^3}\right)^{1/2}, \tag{A2}$$

where the symbols have been defined previously (§ 3). Taking advantage of the fact that the H/He discontinuity is very high in the star in terms of x (i.e., $x \simeq 1$), the integral in equation (A1) reduces to

$$\begin{aligned} \int_d^1 \frac{|N|}{x}\, dx \simeq \int_d^1 |N|\, dx &= \left[(n - \tilde{n}) \frac{GM}{R^3}\right]^{1/2} \int_d^1 \frac{dx}{(1-x)^{1/2}} \\ &= 2\left[(n - \tilde{n}) \frac{GM}{R^3} (1 - d)\right]^{1/2}. \end{aligned} \tag{A3}$$

In the present notation, $d = r_H/R$, and by combining equations (A1) and (A3), we obtain

$$P_{il} = \frac{(2i + n - \frac{1}{2})\pi^2}{2(n - \tilde{n})^{1/2}} \left[l(l+1)\left(1 - \frac{r_H}{R}\right) \frac{GM}{R^3}\right]^{-1/2}. \tag{A4}$$

We thus recover the same functional form as our semianalytic formula (17). In addition, we obtain estimates of the trapping coefficients given by

$$\lambda_i = \left(i + \frac{n}{2} - \frac{1}{4}\right) \frac{\pi}{2(n - \tilde{n})^{1/2}}. \tag{A5}$$

These are the *same* as those obtained from the trapping condition (15) in the asymptotic limit of large values of the argument of the Bessel functions. Indeed, equation (15) gives

$$J_n(x_i) = 0\,. \tag{A6}$$

For large values of x_i,

$$J_n(x_i) \propto \cos\left(x_i - \frac{n\pi}{2} - \frac{\pi}{4}\right), \tag{A7}$$

and the zeros are then given by

$$x_i = \left(i + \frac{n}{2} - \frac{1}{4}\right)\pi . \tag{A8}$$

Combining this with the definition of the trapping coefficient given in § 3, we find

$$\lambda_i = \left(i + \frac{n}{2} - \frac{1}{4}\right)\frac{\pi}{2(n-\tilde{n})^{1/2}} , \tag{A9}$$

which is indeed the same as equation (A5).

For the example given in § 3, $n = 2.5$, $\Gamma_1 = 5/3$, $\tilde{n} = 2.1$, we find from equation (A9) that $\lambda_1 = 4.97$, $\lambda_2 = 7.45$, $\lambda_3 = 9.94$, etc. The values quoted in the text are slightly different because the exact zeros of $J_n(x_i)$ were used there, not the zeros derived from the asymptotic expansion appropriate for $x_i \gg 1$.

APPENDIX B
CHANCE OCCURRENCES IN THE FREQUENCY SPECTRUM OF THE REFERENCE MODEL

An analysis of the eigenvalue spectrum (expressed in terms of *frequency*) of the trapped modes of our reference model leads to a very interesting result. Indeed, in the pioneering work of McGraw (1977), it was first pointed out that the frequencies of many excited modes observed in ZZ Ceti stars can often be expressed as linear combinations of other frequencies present in the spectrum. Specifically, the frequency f of a mode can often be written (within the resolution of the run) as

$$f = mf_i + nf_j , \tag{B1}$$

where m and n are integers and f_i and f_j are the frequencies of two other observed modes. These puzzling relationships have repeatedly been found in other ZZ Ceti stars which have been discovered since McGraw (1977). Nonlinear superposition of modes is known to give rise to harmonics and cross-frequencies (cf. Brickhill 1991), but the expected correlation between the amplitudes of the frequency components is not always observed. Although there is little doubt that some nonlinear effects are indeed present in the Fourier spectra of the large-amplitude ZZ Ceti stars, they may not hold the full story.

We present here an alternative explanation which has the advantage of being extremely simple: the relatively sparse frequency spectrum of the trapped modes of a ZZ Ceti star model is *still* sufficiently dense that accidental occurrences can satisfactorily account for the linear combinations described above. For example, we can easily reproduce to a high level of accuracy *all* of the low-frequency modes of our reference model in terms of linear combinations involving two other frequencies belonging to the spectrum. This is shown in Table 11, where, in terms of the indices l and i, we first give (col. [3]) the frequency spectrum of the

TABLE 11

CHANCE OCCURRENCES IN FREQUENCY SPECTRUM OF REFERENCE MODEL

l (1)	i (2)	f_{li} (mHz) (3)	Frequency Resulting from Linear Combination (mHz) (4)
1	1	$f_{11} = 1.817$	$f_{11} \simeq f_{24} + f_{25} = 1.820$
1	2	$f_{12} = 0.966$	...
1	3	$f_{13} = 0.731$	...
2	1	$f_{21} = 3.212$	$f_{21} \simeq f_{23} + 2f_{12} = 3.214$
2	2	$f_{22} = 1.701$	$f_{22} \simeq f_{25} + f_{37} = 1.701$
2	3	$f_{23} = 1.282$	...
2	4	$f_{24} = 1.002$	...
2	5	$f_{25} = 0.818$	...
2	6	$f_{26} = 0.720$	...
3	1	$f_{31} = 4.474$	$f_{31} \simeq 3f_{35} + f_{12} = 4.479$ $\simeq 2f_{33} + f_{37} = 4.469$
3	2	$f_{32} = 2.372$	$f_{32} \simeq f_{13} + 2f_{25} = 2.367$
3	3	$f_{33} = 1.793$	$f_{33} \simeq f_{12} + f_{25} = 1.784$
3	4	$f_{34} = 1.437$	$f_{34} \simeq 2f_{26} = 1.440$
3	5	$f_{35} = 1.171$	...
3	6	$f_{36} = 1.009$	...
3	7	$f_{37} = 0.883$	...
3	8	$f_{38} = 0.772$	...

trapped modes in our reference model. We recall here that these modes have periods less than or equal to 1400 s, and belong to sequences with $l = 1$, 2, and 3. Column (4) gives frequencies resulting from linear combinations of two other frequencies (other combinations may be possible). Note that, in all cases, we recover the primary frequency to an accuracy better than 0.01 mHz. To obtain such a resolution, it would be necessary to observe a ZZ Ceti star continuously for about 27.8 hr, which, of course, is much longer than any possible run at a single site. In particular, the typical resolution (0.09–0.14 mHz) of discovery runs for new ZZ Ceti stars certainly increases the chance of obtaining acceptable combinations (within the measurement errors). Considering also the possibility that modes other than (and in addition to) trapped modes could be excited in ZZ Ceti pulsators, we find that the frequency spectrum is more than dense enough to explain these linear combinations. We thus conclude that the intriguing frequency numerology observed in the g-mode spectra of ZZ Ceti star could be partly accidental and may not have a physical basis.

REFERENCES

Bergeron, P., Wesemael, F., & Fontaine, G. 1992, ApJ, in press
Berthomieu, G., & Provost, J. 1988, in IAU Symp. 123, Advances in Helio- and Asteroseismology, ed. J. Christensen-Dalsgaard & S. Frandsen (Dordrecht: Reidel), 121
Böhm-Vitense, E. 1958, Z. Astrophys., 46, 108
Bradley, P. A., & Winget, D. E. 1991, ApJS, 75, 463
Brassard, P., Fontaine, G., Pelletier, C., & Wesemael, F. 1991c, in Proc. 7th European Workshop on White Dwarfs, ed. G. Vauclair & E. M. Sion (NATO ASI Series), 193
Brassard, P., Fontaine, G., Wesemael, F., Kawaler, S. D., & Tassoul, M. 1991a, ApJ, 367, 601 (Paper I)
Brassard, P., Fontaine, G., Wesemael, F., & Tassoul, M. 1991d, in preparation
Brassard, P., Pelletier, C., Fontaine, G., & Wesemael, F. 1992, ApJS, in press
Brassard, P., Wesemael, F., & Fontaine, G. 1991b, in preparation
Brickhill, A. J. 1975, MNRAS, 170, 405
———. 1991, preprint
Cox, J. P. 1980, Theory of Stellar Pulsations (Princeton: Princeton Univ. Press)
Cox, J. P., & Giuli, R. T. 1968, Principles of Stellar Structure (New York: Gordon & Breach)
Daou, D., Wesemael, F., Bergeron, P., Fontaine, G., & Holdberg, J. B. 1990, ApJ, 364, 242
Dolez, N., & Vauclair, G. 1981, A&A, 102, 375
Dziembowski, W. 1971, Acta Astron., 21, 289
———. 1977, Acta Astron., 27, 1
Fontaine, G., Bergeron, P., Vauclair, G., Brassard, P., Wesemael, F., Kawaler, S. D., Grauer, A. D., & Winget, D. E. 1991b, ApJ, 378, L49
Fontaine, G., Brassard, P., Wesemael, F., & Tassoul, M. 1991a, in Confrontation between Stellar Pulsation and Evolution, ed. E. Cacciari & G. Clementini (ASP Conf. Ser., Vol. 11), 574
Fontaine, G., & Van Horn, H. M. 1976, ApJS, 31, 467
Hansen, C. J., Kawaler, S. D., & Winget, D. E. 1985, ApJ, 297, 544
Kawaler, S. D. 1986, Ph.D. thesis, Univ. Texas at Austin
———. 1988, in IAU Symp. 123, Advances in Helio- and Asteroseismology, ed. J. Christensen-Dalsgaard & S. Frandsen (Dordrecht: Reidel), 329
Kawaler, S. D. 1991, in Confrontation between Stellar Pulsation and Evolution, ed. E. Cacciari & G. Clementini (ASP Conf. Ser., Vol. 11), 494
Kawaler, S. D., Hansen, C. J., & Winget, D. E. 1985, ApJ, 295, 547
Kawaler, S. D., & Weiss, P. 1991, in Progress of Seismology of the Sun and Stars (Proc. Oji International Seminar), ed. Y. Osaki & H. Shibahashi (Berlin: Springer-Verlag), in press
Lamontagne, R., Wesemael, F., & Fontaine, G. 1987, in IAU Colloq. 95, The Second Conference on Faint Blue Stars, ed. A. G. D. Philip, D. S. Hayes, & J. Liebert (Schenectady: Davis), 677
McGraw, J. T. 1977, Ph.D. thesis, Univ. Texas at Austin
Nather, R. E., Winget, D. E., Clemens, J. C., Hansen, C. J., & Hine, B. P. 1990, ApJ, 361, 309
Press, W. H., Flannery, B. P., Teukolsky, S. A., & Vetterling, W. T. 1986, Numerical Recipes (Cambridge: Cambridge Univ. Press)
Saio, H., & Cox, J. P. 1980, ApJ, 236, 549
Schutz, B. F. 1980, MNRAS, 192, 503
Tassoul, M. 1980, ApJS, 43, 469
Tassoul, M., Fontaine, G., & Winget, D. E. 1990, ApJS, 72, 335
Unno, W., Osaki, Y., Ando, H., Saio, H., & Shibahashi, H. 1989, Nonradial Oscillations of Stars (2d ed.; Tokyo: Univ. Tokyo Press)
Wesemael, F., Bergeron, P., Fontaine, G., & Lamontagne, R. 1991, in Proc. 7th European Workshop on White Dwarfs, ed. G. Vauclair & E. M. Sion (NATO ASI Series), 159
Wesemael, F., Lamontagne, R., & Fontaine, G. 1986, AJ, 91, 1376
Winget, D. E. 1981, Ph.D. thesis, Univ. Rochester
Winget, D. E., & Fontaine, G. 1982, in Pulsations in Classical and Cataclysmic Variable Stars, ed. J. P. Cox & C. J. Hansen (Boulder: Univ. Colorado Press), 46
Winget, D. E., et al. 1991, ApJ, 378, 326
Winget, D. E., Van Horn, H. M., & Hansen, C. J. 1981, ApJ, 245, L33
Winget, D. E., Van Horn, H. M., Tassoul, M., Hansen, C. J., Fontaine, G., & Carroll, B. W. 1982, ApJ, 252, L65
Wood, M. A., & Winget, D. E. 1988, in Proc. Multimode Stellar Pulsation Workshop, ed. G. Kovács, L. Szabados, & B. Szeild (Budapest: Konkoly Observatory), 199